THE STRUCTURAL-FUNCTIONAL NEURAL ARCHITECTURES OF IMPLICIT AND EXPLICIT MOTOR LEARNING

Corson N. Areshenkoff*
Centre for Neuroscience Studies
Department of Psychology
Queens University
Kingston ON, Canada

Anouk J. de Brouwer
Centre for Neuroscience Studies
Queens University
Kingston ON, Canada

Daniel J. Gale
Centre for Neuroscience Studies
Queens University
Kingston ON, Canada

Joseph Y. Nashed
Centre for Neuroscience Studies
Queens University
Kingston ON, Canada

Jonathan Smallwood
Department of Psychology
Queens University
Kingston ON, Canada

J. Randall Flanagan
Centre for Neuroscience Studies
Department of Psychology
Queens University
Kingston ON, Canada

Jason P. Gallivan
Centre for Neuroscience Studies
Department of Psychology
Department of Biomedical and Molecular Sciences
Queens University
Kingston ON, Canada

ABSTRACT

The ability of the central nervous system to learn new mappings between motor commands and sensory feedback is critical for adaptive behaviour. Substantial behavioral evidence indicates that such learning is supported by two distinct, parallel processes: a non-conscious (implicit) process that adapts gradually and a strategic (explicit) process that adapts rapidly. Because behavior at any given moment depends on the combination of these two processes, it has been hard to elucidate their neural underpinnings. Here, using human functional MRI, we identify two whole-brain gradients that arise during motor learning, and describe the relationship between the motor cortex and other regions that are differentially associated with implicit and explicit processes during error-based motor learning. We then show that the activity of the explicit, but not implicit, connectivity gradient in a separate reward-based task predicts learning in the same subjects. Finally, we show that these two learning-related connectivity gradients can be singly explained as opposing ends of a principal axis of macroscale structural-functional cortical organization.

Keywords Motor learning, Reinforcement learning, Functional connectivity, Brain network

*Corresponding author (c.areshenkoff@queensu.ca)

Many of our daily actions stem from the intricate interplay of different mental processes that work in tandem to achieve our intended goals. Broadly, these mental processes can be distinguished by the nature of their cognitive demands: Explicit processes involve conscious mental operations, often requiring our directed attention and deliberate thought, whereas implicit processes operate automatically and outside our conscious awareness (Daniel, 2000). These two processes have been well studied in psychology and neuroscience, and often collaborate to accomplish a wide range of tasks, from learning a foreign language or musical instrument, to driving a car (Ellis, 1993; Gugerty, 1997; Schendan et al., 2003).

In recent years, there has been significant interest in understanding how these two processes support motor learning. For decades, motor learning was widely believed to constitute a singular, implicit process of the sensorimotor system (Wolpert, 1997; Haruno et al., 1998). However, recent behavioral and computational work has demonstrated that motor learning is actually supported by at least two separate learning systems that operate in parallel: a slow-acting implicit system that adapts gradually and a fast-acting explicit system that adapts rapidly (Mazzoni and Krakauer, 2006; Heuer and Hegele, 2008; Hegele and Heuer, 2010; Taylor et al., 2010; Taylor and Ivry, 2011, 2012; Taylor et al., 2014). During visuomotor adaptation tasks, such as when the relationship between hand motion and visual feedback is altered during reaching movements, the explicit system can be revealed by having participants verbally report the direction in which they intend to aim their hand prior to reaching (Taylor et al., 2014). Through subtraction, this verbal reporting procedure is also able to reveal the state of the implicit system, of which the subject is not consciously aware. Recent behavioral work has demonstrated that, whereas the implicit component to learning is fairly stable across participants (Bond and Taylor, 2015; Stark-Inbar et al., 2017; de Brouwer et al., 2018), the explicit strategic component can be quite variable, with subjects who exhibit a larger strategic contribution to learning tending to exhibit faster adaptation (Fernandez-Ruiz et al., 2011; de Brouwer et al., 2018).

While the neural systems that govern these two learning processes are not completely understood, there is evidence from both patient and neuroimaging studies that implicit learning is supported by a network of cerebellar and sensorimotor cortical regions essential for the sensory-guided control of movement (Hardwick et al., 2013; Haar et al., 2015; Kim et al., 2015). By contrast, the neural bases of explicit learning remain far more opaque. Conventionally, explicit learning has been attributed to "task positive" brain areas, such as the dorsolateral prefrontal cortex (DLPFC), that tend to activate across a wide variety of conditions requiring high-level executive processes, spatial working memory, and/or top-down behavioral control (Keisler and Shadmehr, 2010; Anguera et al., 2010; Drummond et al., 2015; Christou et al., 2016; Glasser et al., 2016). Consistent with this attribution, prior work has shown that visuomotor adaptation activates an area of the DLPFC that is also engaged during spatial working memory tasks, with the magnitude of this activity being linked to faster learning (Anguera et al., 2010). Our own work on visuomotor adaptation (Areshenkoff et al., 2022) has corroborated these general findings, showing that faster adaptation is associated with increased functional coupling between areas of the frontoparietal control network and sensorimotor cortex. However, given the strategic nature of explicit learning, it is noteworthy that prior motor learning studies have not commonly focused on activity in

areas of the default mode network, situated at the apex of the cognitive processing hierarchy (Margulies et al., 2016; Smallwood et al., 2021; Paquola et al., 2022).

On the one hand, the lack of DMN activity during studies of motor learning is perhaps not surprising given the "task-negative" nature of these areas (i.e., their tendency to be suppressed during tasks) and having been primarily implicated in more abstract, self-generated cognitive processes (Mesulam, 1998; Spreng et al., 2009; Fox et al., 2015). On the other hand, there is considerable neurophysiological evidence that DMN areas, such as medial prefrontal and posteromedial cortex, are uniquely engaged in conditions when performance is initially poor and when executive control is advantageous (Paulus et al., 2001; Pearson et al., 2011a). For instance, work in nonhuman primates has shown that activity in DMN areas is linked to action exploration and the use of strategies during task performance (Pearson et al., 2011b). This body of work suggests a key role for DMN areas in guiding behavioral adjustments, specifically in the marshalling of cognitive resources when performance errors are high (Pearson et al., 2011a,b).

Consistent with this prior work, contemporary perspectives argue for a broad role of the DMN in task performance, particularly in cases when behaviour must be guided by information accrued over longer time horizons than by in-the-moment sensory inputs (Smallwood et al., 2021). This contribution to behavior is hypothesized to be enabled through the DMN's unique topographic positioning on cortex (Margulies et al., 2016), with each core node of the DMN being located maximally distant from sensory and motor systems. This positioning is thought to free DMN areas from the constraints of extrinsically driven neural activity, allowing them to not only function as the endpoint of a cortical processing hierarchy, but also orchestrate information processing across distributed functional systems (Buckner and Krienen, 2013; Smallwood et al., 2021). Consistent with this neuroanatomical framework, transmodal cortical areas like the DMN exhibit important differences from sensory and motor systems in terms of their anatomical structure. For instance, DMN areas tend to exhibit lower myelin content (Glasser et al., 2014; Stüber et al., 2014; Paquola et al., 2019) but have greater complexity in their patterns of dendritic branching, presumably facilitating the integrative capacity of these regions, as well as their potential for neural plasticity (Teissier and Pierani, 2021). Further evidence indicates that these structural differences are manifestations of an underlying transcriptional architecture, with transmodal brain areas exhibiting a unique pattern of differential gene expression (Hawrylycz et al., 2015). Given these structural-functional features of the DMN, it is possible that the neural basis of explicit learning, rather than being linked to any particular brain region (e.g., DLPFC) or network (e.g., frontoparietal network), is instead a byproduct of transmodal cortex more generally. Indeed, a potentially parsimonious account of the neural substrates of implicit and explicit motor learning is that they simply reflect opposing ends of a whole-brain structural-functional gradient from lower- to higher-order processing systems, and the ways in which these systems interact with motor cortex.

To test these ideas, we exploited a key behavioral feature of explicit motor learning – namely its ability to generalize across different conditions and task contexts (Bond and Taylor, 2015). Prior work has shown that subjects who adopt aiming strategies during error-based learning tasks exhibit better performance in reward-based learning tasks (de Brouwer et al., 2022), which also benefit from the use of explicit strategies (Codol et al., 2018; Holland et al., 2018). Based on these observations, we predicted that whereas the neural systems supporting *implicit* learning are likely to be

tuned to features of the sensory feedback provided by a particular task, the neural systems supporting *explicit* strategic learning are likely to be recruited across different tasks, and predict subject performance. Using functional MRI, we tested this prediction by studying functional connectivity between the primary motor cortex and all other areas of the cortex, basal ganglia, and cerebellum in the same participants during two separate tasks – a visuomotor adaptation task and a reward-based motor task. From the visuomotor adaptation task, we derived whole-brain connectivity gradients that were associated with subjects' explicit aiming strategies and their implicit learning, and then tested whether the expression of the explicit, but not the implicit, learning gradient in the separate reward-based motor task predicted better performance. We then compared our implicit and explicit connectivity gradients to well-established maps of brain structure and function (Markello et al., 2022), examining whether both gradients could be singly explained as the differential expression of a common organizing axis of brain connectivity and microstructure.

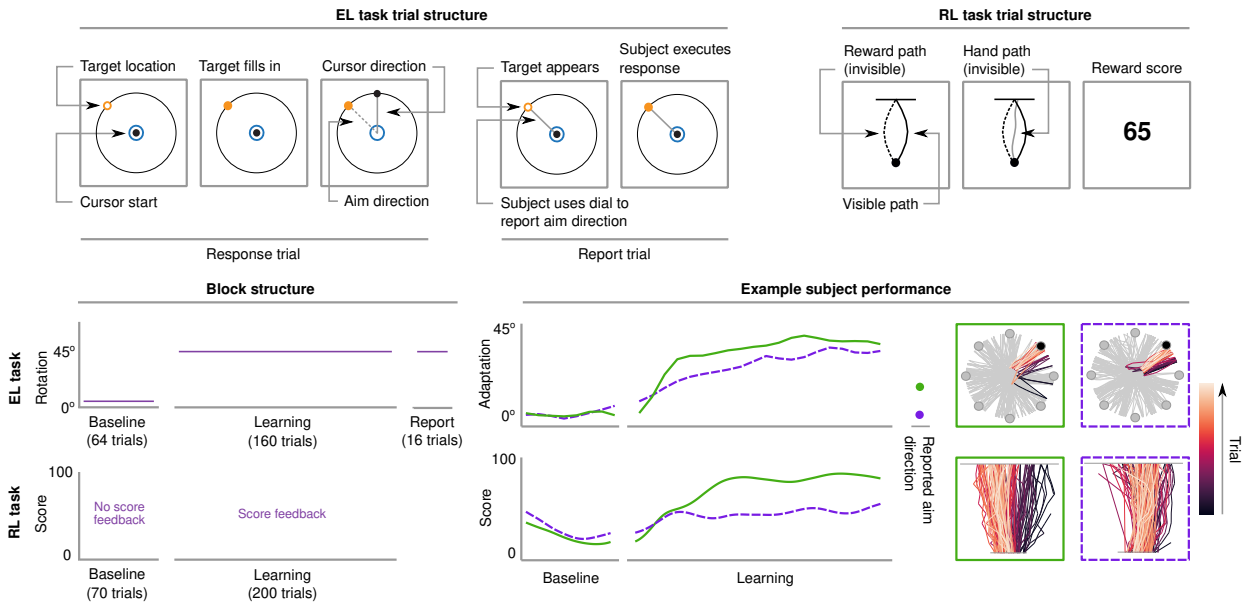

Figure 1: **Motor learning tasks – a)** In the error-based learning (EL) task, subjects performed a standard visuomotor rotation paradigm, wherein they moved a cursor, representing their finger position, from a central starting point to a target on a circular array. During learning trials, we applied a visuomotor rotation so that the cursor moved at an angle of $45°$ relative to the movement of the hand. As such, subjects were required to counteract the rotation (move their hand in the opposite direction) in order to hit the target. At the end of learning, we assayed subjects' conscious knowledge of rotation using a set of report trials in which subjects rotated the position of a dial to report their intended aim direction prior to responding. **b)** In the reward-based learning (RL) task (at top right), subjects were trained to trace a visible, rightward curved path as quickly and accurately as possible, without visual cursor feedback of their finger position. During learning trials, the subject's response was followed by the presentation of score feedback (0 to 100 points), and subjects were instructed to maximize their score across trials. Unbeknownst to the subject, the score presented actually represented their accuracy in tracing a (invisible) mirror image path. **c)** Block structure for the EL and RL tasks. **d)** Example subject data for a faster (green) versus slower (purple) learner in each of the RL and EL tasks, including reported aim direction relative to the target during the EL report block. At the far right are cursor trajectories for individual trials (which were invisible to participants during the RL task). Note that the better learner was able to shift their path towards the rewarded (mirror-image) path in the RL task, and achieved higher accuracy during the EL task.

1 Results

1.1 Learning behavior

In order to study the neural bases of implicit and explicit motor learning, we had subjects (N = 36) perform an error-based learning (EL) task and a reward-based learning (RL) task during two separate MRI testing sessions, one week apart. Both tasks required the subject to move a cursor, representing their finger position, to intercept a target using an MRI-compatible touchpad, subject to different forms of visual feedback. Illustrations of both tasks, as well as typical subject performance, are shown in Figure 1.

In the EL task, subjects performed a classic visuomotor rotation task (Krakauer, 2009), wherein they performed center-out directed movements, using their right finger, towards a target that could appear in one of eight locations on a circular ring. After a baseline block (40 trials), subjects performed a learning block (160 trials) in which the correspondence between finger motion on the touchpad and movement of the cursor was rotated clockwise by $45°$.

Thus, subjects needed to learn to adapt their movements by applying a $45°$ counter-clockwise rotation in order to hit the target. At the conclusion of each trial, subjects received visual (error) feedback consisting of both the target location, as well as the position of their cursor on the target ring. Following the learning block, subjects performed 16 "report" trials (Taylor et al., 2014), in which they were asked to indicate their aim direction using a dial, controlled by their left hand, prior to executing a target-directed movement via their right hand. These report trials were presented at the end of the task, after learning had taken place, in order to avoid drawing attention to the nature of the manipulation and thus biasing subjects' learning behaviour (de Brouwer et al., 2018). Critically, these report trials provided us with an index of subjects' explicit knowledge of, and strategy in counteracting, the visuomotor rotation (Taylor et al., 2014).

In the RL task, we used a modified version of a motor learning task inspired by past work Wu et al. (2014); Dam et al. (2013), wherein subjects used their right finger on the touchpad to trace – *without visual feedback of their cursor* – a rightward-curved path (from a start position to target line). Following a baseline block (70 trials), in which subjects did not receive any feedback about their performance, they performed a learning block (200 trials). Here, they were instructed that they would now receive score feedback, between 0 and 100, based on how accurately they traced the visible rightward-curved path, and that they should attempt to maximize their score across trials. Critically – and unbeknownst to the subjects – the score they received was *actually* based on how accurately they traced the mirror-image path (reflected across the vertical axis). As the cursor was invisible, subjects had only the score feedback (and thus no error-related directional information) with which to refine their movements across trials.

Behavioral data associated with the two motor learning tasks are shown in Figure 2. For each subject, we obtained learning trajectories by recording the adaptation on each trial of the EL task (defined as the hand direction relative to the target) and the score obtained on each trial of the RL task. Mean performance and individual subject learning curves are shown in Figure 2a, confirming that subjects, on average, successfully learned each task. However, these group-averaged results are potentially misleading, as they obscure significant inter-subject variability in both the rate and extent of learning in each task. To summarize these inter-subject differences in a data-driven manner, we performed functional principal component analysis (fPCA; Shang, 2014) on subjects' learning curves (see Methods). These components are shown in Figure 2b, while individual component scores are shown in Figure 3. For each task, we found that a single component, encoding overall learning, captured the majority (75%) of variability in individual subjects' learning curves. Thus, these learning performance scores formed the basis of our analyses moving forward.

In the EL task, we observed a large degree of variability in subjects' aiming directions during the report trials, ranging from zero explicit knowledge (wherein subjects reported aiming directly at the target) to complete compensation (i.e., wherein subjects aimed $45°$ to fully counteract the imposed rotation). Consistent with our prior work (de Brouwer et al., 2018, 2022), and the notion that explicit strategy use is associated with better overall learning performance, we found that subjects who reported larger aiming directions learned better at the task 3a ($r = 0.37$, $t_{34} = 2.33$, $p = 0.026$). Given this relationship, as well as prior evidence that motor RL performance relies strongly on explicit processes (Holland et al., 2018; de Brouwer et al., 2022), we next wondered whether subject performance in the EL task could predict performance in the separate RL task. Although here we only observed a modest positive correlation between

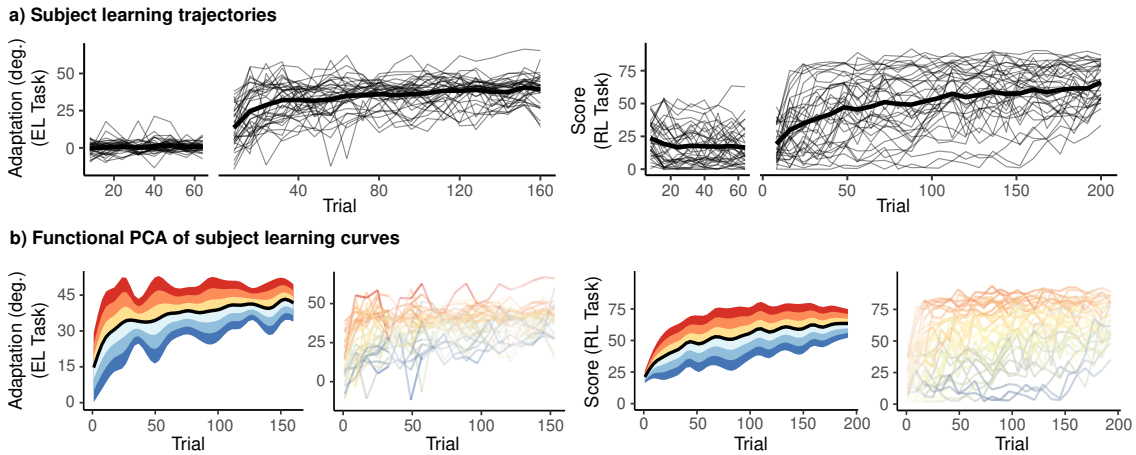

Figure 2: **Subject learning behavior – (a)** Individual subject learning curves for the EL (left) and RL (right) tasks. Solid black lines denote means across all subjects (N=36). **b)** We performed functional principal component analysis on subjects' learning curves in each task in order to identify the dominant patterns of variability. In both cases, a single component – encoding overall learning – explained a majority of the observed variance. Left panels show the top component, with red (resp. blue) bands denoting the effect of positive (resp. negative) scores, relative to mean performance. In both tasks, the top component encoded overall task performance (better or worse than average). Right panels show individual subject learning curves, colored by subjects' score on the top component.

performance in the two tasks ($r = .11$, t_{34}, $p = .5$), further inspection revealed that this relationship was mediated by subjects' use of cognitive strategies. Specifically, among subjects who reported using a re-aiming strategy during the EL task, we found that performance across the two tasks was highly correlated; conversely, among subjects who reported no explicit knowledge of the rotation, we observed zero correlation between EL and RL performance. For a visualization of this effect, Figure 3b (top) shows the association between EL and RL performance based on a median split of subjects' explicit reports, indicating a clear positive relationship in highly explicit subjects, and no relationship for subjects reporting little explicit knowledge. To quantify this effect, we fit a Bayesian multivariate regression model in which both EL and RL task performance, as well as the correlation between them, varied as a function of subjects' explicit reports (see Methods for details). This analysis revealed a clear positive effect of explicit strategy use on the correlation between EL and RL task performance (Figure 3b).

A clear implication of the above behavioural results is that RL performance, and the EL performance of subjects who use explicit strategies during learning, are supported by a common explicit, strategic process. Thus, a specific neural prediction is that the patterns of functional connectivity associated with explicit learning during EL should similarly predict better performance during the RL task. Conversely, subjects who do not report knowledge of the rotation in the EL task presumably rely more strongly on implicit adaptation. Because this form of learning in the EL task is driven primarily by sensory prediction errors that are unavailable during RL, we would also predict that the patterns of connectivity associated with *implicit* EL learning should not predict subject RL performance.

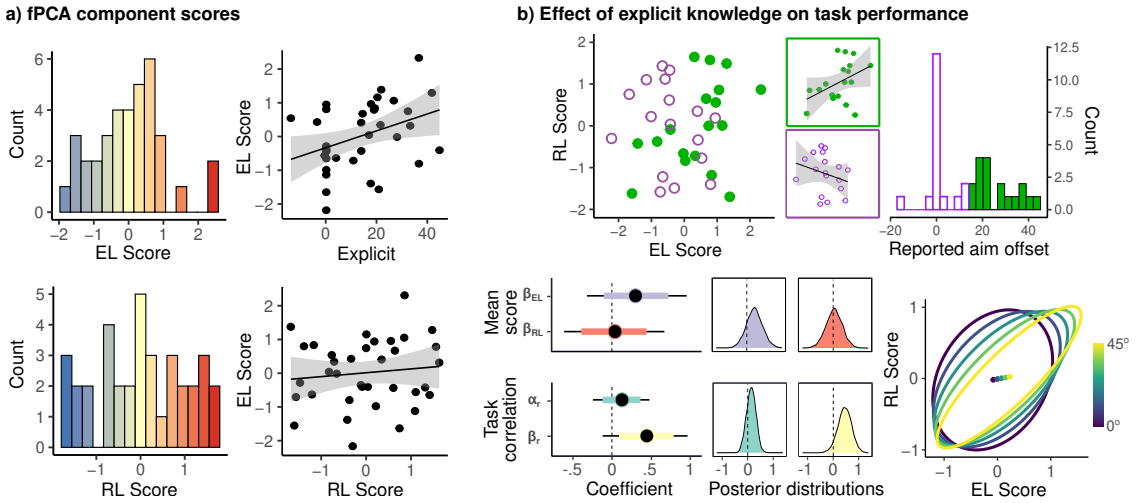

Figure 3: **Relationship between explicit learning and subject performance in both tasks– a)** (left) Histograms of subjects' scores on the EL and RL behavioral components. (right top) Subjects reporting explicit knowledge of the rotation exhibited greater performance in the EL task. (right bottom) Relationship between EL and RL task performance. **b)** (top) Relationship between EL and RL task performance following a median split of subjects by their explicit reports. Among highly explicit subjects (green), performance in the EL and RL tasks was highly positively correlated (see inset scatterplots). (bottom) We constructed a Bayesian multivariate regression model in which EL and RL performance, as well as the error covariance, varied as a function of subjects' reported aim direction. Left panel shows posterior means (black dots) and highest posterior density intervals (thick and thin lines, 50% and 90% respectively). Top intervals are standardized coefficients for the effects of explicit knowledge on mean EL and RL performance. Bottom intervals are the intercept and slope for the effect of explicit knowledge on the (Fisher transformed) correlation. (middle panel) Posterior distributions for the parameters just described. (right panel) Posterior mean predicted distributions of EL and RL scores as a function of reported aim offset. Points denote predicted mean scores, while ellipses represent a Mahalanobis distance of 1.

1.2 Functional connectivity associated with explicit and implicit learning processes

To test our above neural predictions, we examined learning-dependent changes in functional connectivity between the primary motor cortex and the rest of cortex, basal ganglia, and cerebellum during both the EL and RL tasks (Figure 4, top). By constraining our analysis to bipartite functional interactions with primary motor cortex, we were specifically interested in assessing how 'non-motor' regions in cortex, the basal ganglia and cerebellum, modulate their connectivity with cortical areas located in the final motor output pathway that generate motor behaviour. To identify the neural bases of explicit versus implicit learning, we first derived measures of these two learning components for each subject in the EL task: We defined *explicit* learning as the mean difference between subjects' reported aim direction and the target location, and we defined *implicit* learning as the mean difference between subjects' reported and actual aim directions (Taylor et al., 2014). Note that while our goal is to relate each of these learning components to patterns of whole-brain functional connectivity with the motor cortex during task performance, there is the subtle complication that these components are necessarily conflated with differences in subject performance. For instance, as we have shown here, explicit learning is associated with better performance in EL task, and thus it is important that we disentangle neural effects related to explicit strategy use versus effects related to changes in neural activity in response to the reduction of

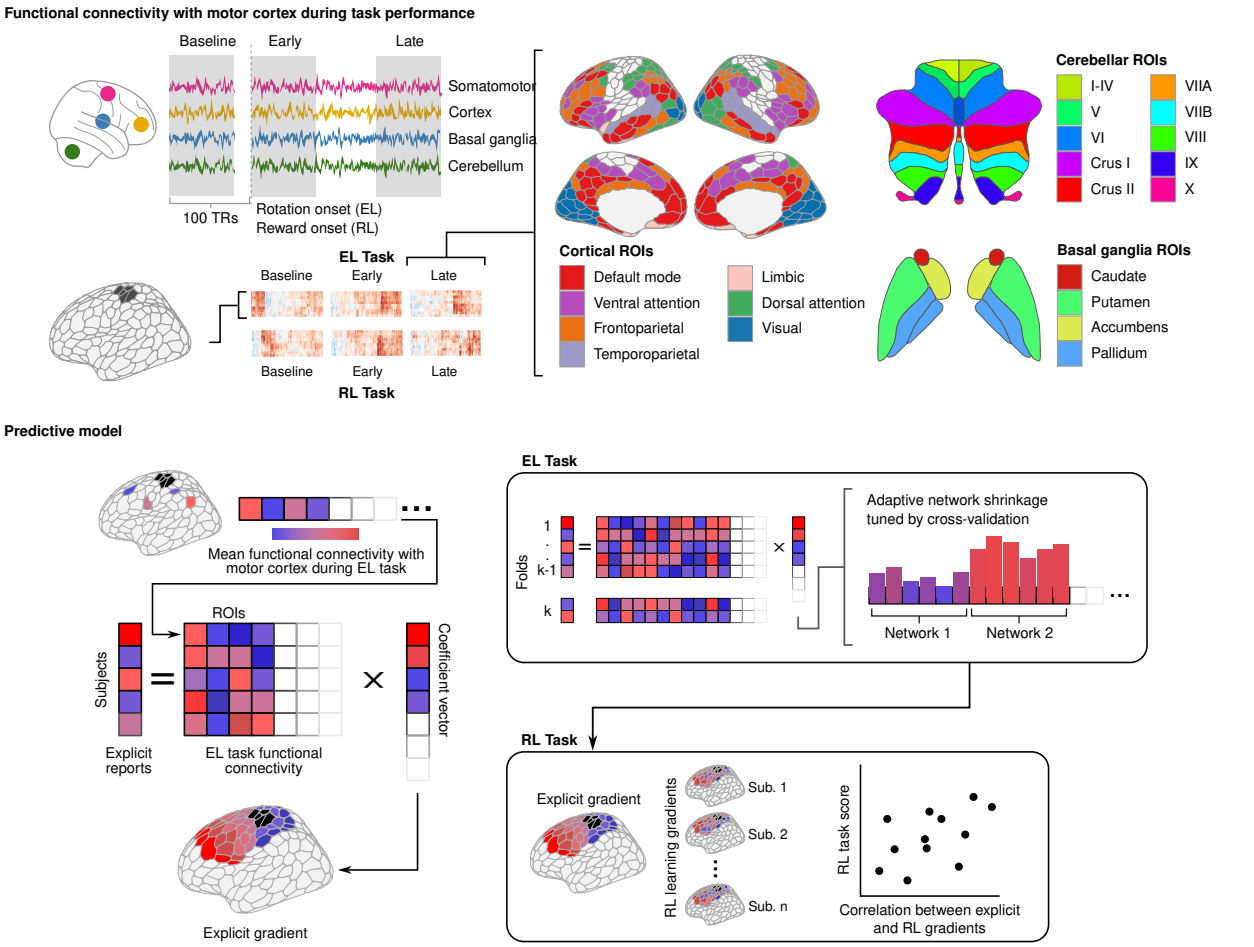

Figure 4: **Neuroimaging and analysis approach (top) –** For each motor learning task, we studied functional connectivity between regions of the left (contralateral) somatomotor cortex, and bilateral functional networks across the entire cortex, basal ganglia and cerebellum. For each region of interest (ROI), we estimated its BOLD signal covariance with the motor cortex during each of the baseline, early and late learning epochs. Cortical ROIs were identified using the 400 region parcellation of Schaefer et al. (2018), and assigned to functional networks based on the 7 network parcellation of Yeo et al. (2011). Cerebellar ROIs were defined based on the parcellation of (Diedrichsen, 2006, ; 28 parcels), while basal ganglia ROIs were defined using the Harvard-Oxford parcellation (Frazier et al., 2005; Makris et al., 2006, ; 8 parcels). **Schematic diagram of our predictive model (bottom) –** We fit penalized regression models predicting subjects explicit and implicit EL task scores using the mean functional connectivity of each non-motor ROI with the motor cortex. We used the group-penalized ridge regression model proposed by Van De Wiel et al. (2016), with separate shrinkage parameters for each of the cortical networks, as well as the basal ganglia and cerebellum. These parameters were tuned using leave-on-out cross validation on subjects' EL task data. We then correlated the resulting coefficient vectors with functional connectivity estimated from each subject during the RL task.

visuomotor errors. Thus, for our analysis of subjects' explicit learning data, we included subjects' EL task scores as a covariate in order to control for subjects' performance (see Methods for further details on this approach).

To perform our neural analyses, we extracted fMRI timecourse activity from the cerebellum, striatum and all of cortex (except for the cortical somatomotor network), and studied functional connectivity between these regions and the average activity of a subset of 4 regions in the left (contralateral) hemisphere comprising the hand motor region (belonging to the left Somatomotor A network Schaefer et al. (2018). For each subject, we estimated covariance networks during the baseline and learning scans in each of the EL and RL tasks. During the learning epoch, we extracted timecourse activity

from both early and late learning periods (defined as the first and last 100 imaging volumes), allowing us to describe changes in connectivity over the course of learning. As described in the Methods, we centered each subjects' covariance matrices to remove overall mean differences in functional connectivity, which we have shown can significantly obscure task-related effects (Areshenkoff et al., 2022). As a result, note that our effects reflect task-related differences in covariance *relative to the average*. See Methods for full details.

Using the patterns of functional connectivity extracted from the early learning phase (where the contributions of explicit learning to performance are most prominent; de Brouwer et al., 2018; Taylor et al., 2014), we predicted subjects' explicit and implicit learning during the EL task using a group-penalized ridge regression model (Van De Wiel et al., 2016) with separate shrinkage parameters for each of the cortical networks, basal ganglia and cerebellum (see Figure 4, bottom). The coefficients from this model create connectivity gradients (reflecting covariance with motor cortex) that span the cortex, basal ganglia, and cerebellum, which we hereby refer to as the *explicit* and *implicit* learning gradients. Note that, in order to control for the association between explicit learning and performance (noted above), the predictive model for subjects' explicit scores was fit to the residuals after regressing out subjects' EL task scores (see Methods for details).

Surface maps for the explicit and implicit connectivity gradients associated with the early learning phase are shown in Figure 5. Within the implicit gradient, we observed the highest regional loadings in the dorsal attention network, comprising premotor and parietal regions known to support motor learning and control (Scott, 2012; Hardwick et al., 2013). By contrast, within the explicit gradient, we observed the highest regional loadings within the default mode and limbic networks (see barplots in Figure 5, right).

Note that it is difficult to directly compare these gradients, as they are produced by models fit to separate (albeit inversely related) outcome measures (i.e., our measures of implicit versus explicit learning). We thus derived a single brain map – the *explicit alignment gradient* – by computing the difference in rank for each ROI, such that positive values indicate relatively greater loading on the explicit, compared to implicit, gradient (Figure 5, bottom). In this brain map, a positive loading region can be described as being *explicit aligned*, indicating that the region is more associated with explicit compared to implicit learning (and vice versa for *implicit aligned* regions). As can be seen in Fig 5 (bottom right), the greatest explicit alignment was seen in default mode subnetwork B (the dorsal-medial subnetwork), limbic subnetwork B (the temporal poles), and ventral attention subnetwork B, and the least explicit (most implicit) alignment was observed in the dorsal attention subnetwork B. Together, these findings support the view that explicit learning is supported by several areas distributed across higher-order transmodal cortex whereas implicit learning is supported by more localized, sensorimotor areas within premotor and superior parietal cortex.

1.3 Task-specific implicit and task-general explicit learning systems

Having established the whole-brain patterns of connectivity associated with implicit and explicit learning in the EL task, we next tested our specific neural prediction that the expression of the explicit, but not implicit, gradient in the separate RL task would predict subjects' performance in that separate task. In order to quantify the expression of these two connectivity gradients during RL task performance, we computed the correlation between each gradient and subjects'

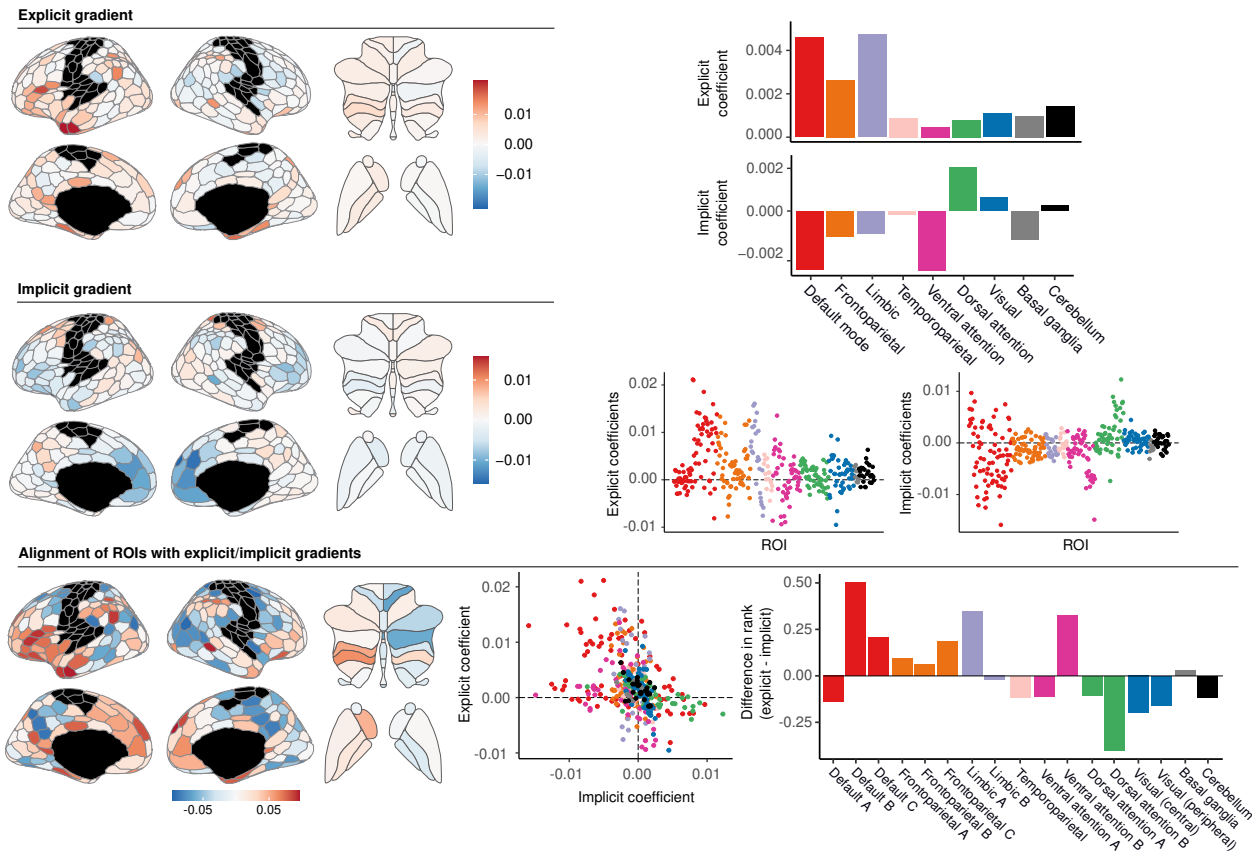

Figure 5: **Surface maps for the explicit and implicit connectivity gradients – a** Model coefficients for each ROI in the explicit and implicit learning gradients. Barplots denote the mean coefficient for each cortical network defined by Yeo et al. (2011), along with the cerebellum and striatum regions. Traceplots at bottom denote coefficients for each individual ROI. **b)** Surface maps for the explicit alignment gradient, denoting the difference in rank for each ROI (explicit - implicit). Scatterplot displays implicit and explicit coefficients for each ROI. Barplot displays mean coefficient broken down by subnetwork.

pattern of functional connectivity expressed during the early learning epoch of the RL task. The results of this approach are two separate weightings – one for each gradient – reflecting the degree to which subjects expressed patterns of functional connectivity associated with explicit or implicit learning – as estimated from the EL task – during RL task performance.

Consistent with the notion that the explicit learning gradient reflects the recruitment of task-general strategic processes, we found that the expression of this gradient during the early learning epoch of the RL task was correlated with subjects' RL performance ($r = .35$, $t_{34} = 2.14$, $p = 0.039$, $\text{CI}_{95} = [0.02, 0.6]$). Conversely, the expression of the *implicit* gradient was not ($r = -0.13$, $t_{34} = -0.79$, $p = 0.43$, $\text{CI}_{95} = [-0.44, 0.2]$). Note that, although this difference in correlation was quite large, it was not, itself, significant ($r_{\text{exp}} - r_{\text{imp}} = 0.48$, $z = 1.75$, $p = 0.08$; Pearson and Filon, 1898).

As a set of control analyses, we next sought to understand the specificity of these above effects. First, one possibility is that the patterns of connectivity that characterize our explicit gradient may not uniquely reflect functional interactions

with the contralateral hand area of motor cortex (the primary output pathway for motor adjustments in our task), but instead reflect a much larger pattern of functional connectivity with somatomotor cortex more generally. To test this, we repeated our above analyses but instead of using the contralateral hand motor area, we used the ipsilateral hand area, as well as bilateral motor regions active during tongue movement (Schaefer et al., 2018). Notably, in each of these cases, we observed no correlation of the derived implicit and explicit gradients with RL performance (Figure 6; left).

A second possibility is that our effects may have nothing to do with learning *per se*, but instead reflect differences in the way that subjects approach performance in the tasks (e.g., differences in focus), or alternatively, baseline differences in functional connectivity that are subsequently predictive of explicit strategy use. Such explanations are indeed plausible, as individual differences in executive functions have been associated with differences in resting state functional connectivity (Reineberg et al., 2015), and executive functions have, in turn, been linked to motor learning processes (Ludyga et al., 2019). Thus, it is possible that connectivity gradients derived during the baseline epoch, or even during the late learning epoch, might also correlate with RL task performance. However, when we reproduced our entire analyses using activity from these other epochs, we found that this was not the case; a significant correlation between the explicit gradient and RL performance was observed only during the early learning epoch (Figure 6; center).

Finally, our decision to control for EL task performance when deriving our explicit gradient could be contested on the grounds that the causal effects of explicit learning and neural activity on performance risk introducing collider bias when EL performance is controlled for (Cole et al., 2010). Although this possibility cannot be ruled out statistically, as an additional approach we derived two additional gradients: One derived from subjects' uncorrected explicit reports, and the other using subjects' EL task scores. Notably, we observed zero correlation between the latter EL *performance* gradient and RL performance ($r = -0.01$, $t_{34} = -0.06$, $p = 0.96$, $\text{CI}_{95} = [-0.34, 0.32]$). In contrast, the *uncorrected* explicit gradient was essentially identical to the corrected version, though non-significant ($r = 0.32$, $t_{34} = 1.96$, $p = 0.058$, $\text{CI}_{95} = [-0.34, 0.32]$).

Taken together, the above analyses suggest that it is the expression of the EL-derived explicit, and not implicit, gradient during the RL task that predicts RL performance. Moreover, our control analyses demonstrate that (1) this relationship is specific to the early learning phase of the task, when cognitive strategies exert their largest effects on performance (Taylor et al., 2014; de Brouwer et al., 2018), and, (2) it reflects selective changes in functional connectivity with contralateral motor cortex. Moreover, this effect was driven by subjects' use of strategies and not by performance *per se*, as no such predictive ability was seen when a gradient was derived from subjects' EL task scores.

1.4 Explicit and implicit learning gradients constitutes opposing ends of a principal structural-functional axis of cortical organization

Lastly, we wondered the extent to which the explicit and implicit learning gradients identified in our study correspond to known structural and functional gradients of cortical organization documented in previous MRI, MEG, PET and microarray gene expression studies. To this end, we used the neuromaps toolbox (Markello et al., 2022) to compare our explicit alignment gradient 5 to a set of 23 target maps capturing a range of structural, molecular, temporal and

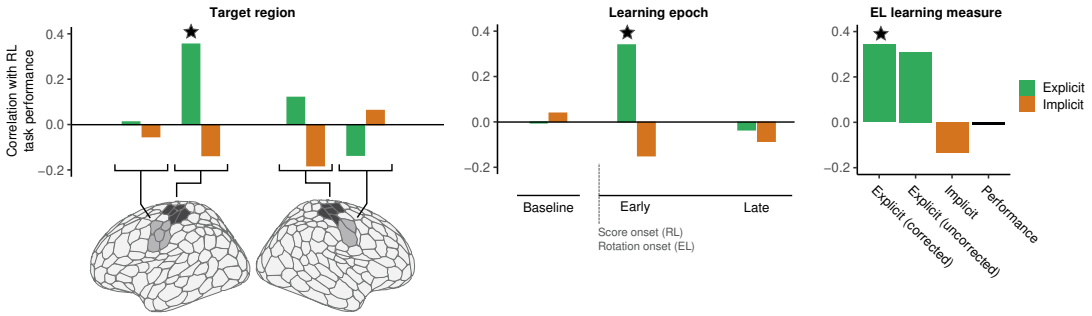

Figure 6: **The relationship between RL task performance and the expression of the explicit/implicit learning gradients –)** We correlated our explicit and implicit connectivity gradients, derived from the EL task, with subjects' functional connectivity exhibited during the learning epoch of the RL task. The resulting correlation values were then correlated with subjects' RL task performance. As a set of control analyses, we repeated this analysis for the ipsilateral hand region of the (right) motor cortex, as well as bilateral tongue regions of motor cortex (gray parcels in gray). We also repeated the analysis during the baseline and late learning epochs (center). Finally (right), we derived gradients based on subjects' EL task performance, as well as for uncorrected explicit reports. Note that significant predictive ability (stars) was only seen for the explicit gradient, only during the early learning epoch, and only when considering functional connectivity with the contralateral hand area of motor cortex.

functional features of cortex, and tested for statistical significance (with Pearson's r) using a spatial autocorrelation-preserving null model ('spin test')(e.g. Markello et al., 2022). As shown in Figure 7, we observed significant positive correlations between our explicit alignment gradient and features of cortical function, including: (1) the principal gradient derived by Margulies et al. (2016) from resting-state functional connectivity, and (2) high frequency gamma power. In addition, we also observed a significant negative correlation between our explicit alignment gradient and cortical myelin concentration.

In order to better characterize the overall patterns of similarity amongst these gradients, we embedded and clustered the full set of gradients in a common (spherical) space using the angle between by the subspaces spanned by each gradient (allowing us to account for differences in the sign of some of the gradients; see Methods for details). Note that, as our explicit gradient omits the somatomotor networks, we omitted these regions from all gradients prior to performing our comparisons. The results of this embedding analysis are shown in Figure 7 (bottom), along with the results of a hierarchical clustering.

All three functional gradients included in our analysis (explicit alignment, the Margulies et al. principal gradient, and the Neurosynth PC1 cognitive gradient) were grouped within a single cluster (green), along with cortical gamma and delta power. Note the latter two functional gradients both comprise roughly unimodal-to-transmodal gradients anchored by the primary sensory and motor regions at one end, and the default mode network at the other. The explicit alignment gradient was positively correlated with each of these, suggesting that the relative alignment of each cortical parcel with explicit and implicit learning processes roughly accords with its position along the unimodal-transmodal principal gradient. The remaining clusters comprised a set of anterior-posterior gradients (red), a set of largely dorsal-ventral gradients (blue), a set of neurotransmitter receptor gradients (purple), and the pair of gradients encoding evolutionary expansion and functional cohomology (black). Together, these results are consistent with the idea that the whole-brain patterns of functional connectivity with motor cortex that are associated with implicit versus explicit learning can be

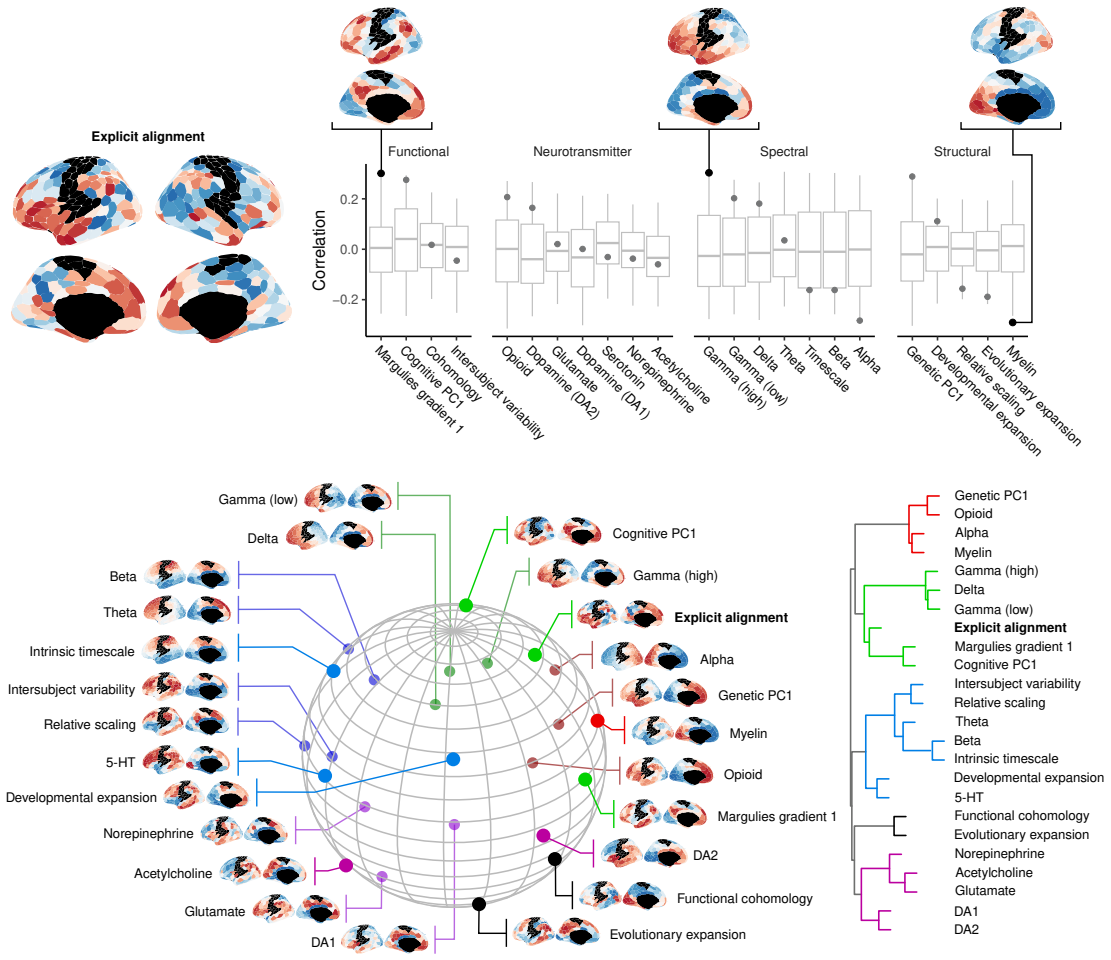

Figure 7: **Relationship between our explicit alignment gradient and other maps of cortical structure and function** – For each brain map, we computed the Pearson correlation with our explicit alignment gradient (black and grey points). Boxplots denote permutation distributions estimated from a spatial autocorrelation-preserving null model. The boxes denote the .25, .5, and .75 quantiles, while whiskers denote the critical values for a two sided test at $\alpha = .05$ (that is, the .025 and .975 quantiles). See methods for a description of each brain map. **(bottom)** We derived a spherical embedding based on the angle between the subspaces spanned by each brain map. Colors denote groups derived from a hierarchical clustering of these gradients (dendrogram displayed on right).

parsimoniously explained as emergent features of a structural-functional cortical processing hierarchy extending from unimodal to transmodal cortex.

2 Discussion

Adaptive behaviour is frequently achieved through a combination of explicit and implicit learning processes, yet the whole-brain architecture that supports these processes, and the extent to which this architecture supports different forms of learning, is poorly understood. Here we examined, in the same human participants, changes in cortical, striatal and cerebellar functional connectivity with primary motor cortex while individuals learned to adjust their motor commands through either sensory errors (EL task) or reward-based feedback (RL task). Using subjects' behavioural reports from the EL task, we isolated gradients of functional connectivity during learning that were associated with the implicit and explicit components of visuomotor adaptation. The implicit learning gradient constituted an increase in functional connectivity between the motor cortex and premotor and superior parietal areas of the dorsal attention network (DAN). By contrast, the explicit learning gradient constituted an increase in functional connectivity between the motor cortex and higher-order regions located in transmodal cortex – including, most prominently, areas of the default mode and limbic networks. Consistent with our behavioural data showing that subjects who used explicit strategies during the EL task performed better during the RL task, we found that it was the expression of the explicit learning gradient, and not the implicit gradient, that predicted subject performance in the RL task. Our control analyses demonstrated that this predictive relationship was exclusive to both the early learning phase of the task, when cognitive strategies are known to exert their largest effects on performance, and to functional connectivity with the contralateral hand region of the motor cortex. Lastly, when we compared our task-derived implicit and explicit learning gradients to other reference maps and biological ontologies of the human brain, we found that these gradients constituted opposing ends of a single macroscale structural-functional cortical gradient, extending from unimodal to transmodal cortex. Together, our findings establish the whole-brain functional architectures of explicit and implicit motor learning and help ground this architecture in a principal axis of cortical organization.

2.1 Composition of the explicit alignment axis

We found that the brain areas with the strongest implicit alignment were located in subnetwork B of the dorsal attention network. This finding is consistent with a large body of modeling and neurophysiological work implicating specific regions of this subnetwork, such as the posterior parietal and premotor cortices, in the sensory guided control of visual-motor behaviour (see Scott, 2012, for a general overview). Indeed, contemporary theories of sensorimotor adaptation, based on optimal feedback control, credit regions of this network in the maintenance and updating of an internal forward model in response to sensory feedback (Scott, 2004). Although we found that the cerebellum loaded relatively weakly onto the implicit gradient, we note that its anterior motor regions, particularly in the right (ipsilateral) cerebellum, were aligned to the implicit gradient, which is consistent with the known role of this structure in computing the sensory prediction errors that drive implicit motor adaptation (Smith et al., 2006; Tseng et al., 2007; Wolpert et al., 2011; Manto et al., 2012; Tanaka et al., 2020).

By contrast, we found that the brain areas with the strongest explicit alignment were located in the default-mode subnetwork B (corresponding to the dorsal-medial subnetwork), limbic subnetwork A, and subnetwork B of the ventral

attention network. In prior work, searches for the neural substrates of explicit motor learning have generally focused on brain regions involved in working memory that are already known to exert direct top-down control over behavior, such as the DLPFC (Liew et al., 2018). However, the explicit re-aiming strategy during visuomotor adaptation also clearly involves long-term memory processes that support the ability to develop high-level contextual models that account for the mapping between motor commands and feedback. For example, a naive subject who responds directly to a rightward target under a clockwise rotation will experience a downward error, and thus may initially (and mistakenly) believe that such an error implies a downward movement of the cursor relative to their aim direction. Thus, when asked to respond to a leftward target on the next trial, they might respond more "upward" (i.e. more clockwise), which is the opposite of the correction necessary to counteract the rotation. As such, learning the correct behaviour for this perturbation requires contextualizing the specific perceptual errors experienced on each trial within a high-level model of the visuomotor transformation (i.e. "the cursor direction is rotated relative to my aim direction" rather than "the cursor moves downward relative to my aim direction"). Learning this mapping requires maintaining action-outcome associations in memory across multiple trials, necessitating neural systems capable of sustained computations over timescales longer than that of a single trial (or even a few trials). There is considerable evidence that successful performance in these contexts – in which responding must be guided by a high-level representation of the task-structure, and by the episodic memory of previous trials – depends on the contribution of networks of regions in association cortex, and the default mode network in particular (Konishi et al., 2015; Murphy et al., 2018, 2019).

In contrast to the classical view that the default mode network (DMN) contributes mainly to mind-wandering and introspective thought during rest, modern perspectives emphasize that the DMN is well suited to support cognition in tasks where responding must be guided by features other than the current sensory input (such as by internally generated rulesets or strategies; Smallwood et al., 2021). This is believed to be enabled by the network's topographic organization on cortex, in which core regions are located maximally distant from primary sensory and motor regions, allowing them broad oversight over whole-brain patterns of activity and the capacity to integrate diverse sources of perceptual and contextual information. In this regard, it is noteworthy that, within the DMN, we observed relatively greater explicit alignment in subnetworks B and C, corresponding roughly to the dorsal-medial and medial-temporal subsystems described by Andrews-Hanna et al. (2010). The latter, medial-temporal subsystem, has in particular been implicated in the recall of task-relevant perceptual and conceptual information from previous trials (Binder et al., 2009), and when performance must be guided by the integration of multiple perceptual features (Kumaran et al., 2009; **?**). Consistent with these functional properties of the DMN, we further show that our explicit alignment gradient was significantly positively correlated with the principal functional gradient identified from Margulies et al. (2016), spanning from unimodal to transmodal cortex. As noted by others (Huntenburg et al., 2018), this architecture closely resembles functional differences in the time horizons over which sensorimotor and transmodal areas process information. Previous research has demonstrated that the temporal windows of information processing change in a hierarchical fashion across cortex (Hasson et al., 2008, 2015; Baldassano et al., 2017), with sensorimotor areas integrating information over the order of milliseconds to seconds versus transmodal areas that integrate information over the order of seconds to minutes

and longer. These longer "temporal receptive windows" in transmodal cortex (Hasson et al., 2008, 2015) are thought to enable these areas to encode more slowly changing states of the world and incorporate acquired knowledge into more complex scenarios -– attributes that are both crucial for successful learning.

This functional framework is also consistent with neural evidence from monkeys linking DMN regions with the encoding of response strategies that span across multiple trials (Pearson et al., 2009), as well as the known role of specific DMN subnetworks (such as subnetwork C) in the use of episodic memory of previous trials to guide current responding (Andrews-Hanna et al., 2010). It is also worth noting that, while the precise functional significance of many cortical oscillations are poorly understood, previous models Harmony (2013) suggest that one effect of increases in cortical delta activity – whose gradient clustered with out explicit alignment axis – is to signal a suppression of afferent sensory signals which would otherwise interfere with ongoing internal processing. This kind of task-dependent gating of incoming sensory information appears to be essential to proper default mode network function, allowing regions of this network to maintain specific, task-relevant information in memory while suppressing irrelevant perceptual inputs Zhang et al. (2019, 2022).

At a structural level, we further found that our explicit alignment axis was inversely correlated with cortical myelin concentration, whereby the lowest levels of myelination are observed in core areas of the DMN (Glasser et al., 2014; Huntenburg et al., 2017). The low myelin content of transmodal cortex presumably reflects the fact that its myelination occurs relatively later during development (Flechsig, 1920), which may predispose these areas toward increased synaptic plasticity (Braitenberg, 1962), thus facilitating adaptive behavior and learning (Huntenburg et al., 2017). This is wholly consistent with the role of these regions in general executive functions, which develop over the course of childhood and adolescence; and in turn, with the association between the development of executive functions and motor coordination (Piek et al., 2004; Martin et al., 2010; Ludyga et al., 2019).

Although comparatively few studies have examined the use of reinforcement mechanisms during motor learning (though see Izawa and Shadmehr, 2011; Therrien et al., 2016; Galea et al., 2015; Doyon et al., 2009), there is emerging behavioural evidence that explicit learning processes are particularly crucial in tasks that deny the sensory feedback supporting error-based adaptation, such as our reinforcement learning task, or the tasks of Holland et al. (2018); de Brouwer et al. (2022); Dam et al. (2013). In these tasks, the agent is provided no feedback indicating precisely how, or to what extent, the executed versus optimal movements differ, and so they must perform some kind of credit assignment in order to decide which feature of the movement to adjust on subsequent trials (Sutton and Barto, 2018). In these contexts, subjects will often develop an explicit understanding of the task structure, and their responses show a clear prioritization of the features relevant to performance (Dam et al., 2013; de Brouwer et al., 2022). For example, although there was no sensory feedback indicating how trajectories should be updated in order to achieve a higher score in our task, subjects overwhelmingly adjusted the leftward/rightwardness of their responses, rather than experimenting with paths of different shapes. Many subjects in turn exhibited periods of abrupt learning, book-ended by relatively flat performance, suggesting a sudden realization of the correct trajectory. These abrupt shifts in behaviour have been studied in the context of one-shot learning, where research has repeatedly implicated frontal regions of the default

mode network (Lee et al., 2015). Moreover, recent work on reinforcement learning has implicated the parahippocampal cortex – a core node of the default mode subnetwork C – in an *episodic control system* which facilitates rapid learning through an explicit record of past action-outcome associations (Doll et al., 2015). As noted above, networks containing these regions were strongly aligned to our explicit gradient derived from the EL task, the expression of which predicted subject performance in the RL task.

2.2 Methodological considerations

For practical reasons, we restricted our analysis to bipartite networks describing functional interactions between the motor cortex and the rest of the brain. We believe this is a sensible restriction, as the motor cortex serves as the primary output pathway in the motor system, and it is functional interactions with this system, in particular, that are thought to result in modifications to behaviour (i.e., learning). Indeed, consistent with this interpretation, we found that the connectivity between transmodal cortex and other non-hand areas of motor cortex could not reliably predict subject performance in the separate RL task. However, a limitation of this targeted, bipartite approach is that we cannot speak to connectivity changes occurring outside of the motor cortex hand area that may also relate to behaviour. Further, it also means that our gradient comparisons (Figure 7) necessarily exclude the somatomotor cortices, which feature prominently in several reference gradient maps.

Our derivation of the explicit learning axis, and by association, the implicit learning axis, was based on subjects' self-reported aim direction during the report block in the EL task. Although this measure has been well validated experimentally, and correlates well with features of performance associated with explicit learning (Taylor et al., 2014; de Brouwer et al., 2018), it is possible that some subjects whom we have characterized as implicit may, in actuality, have simply failed to understand the instructions associated with explicit reporting (thus leaving the report dial pointing at the target location). This likely explains the large performance variability in subjects reporting zero explicit knowledge (Figure **??**c). Nevertheless, given both the existing literature (Taylor et al., 2014; de Brouwer et al., 2018; **?**) and the fact that we observe a clear relationship between performance and reported aim direction among subjects reporting a non-zero re-aiming direction, we believe that subjects' reports provide a valid, albeit noisy, metric of explicit strategy use.

Finally, although we included regions of both the basal ganglia and cerebellum in our analysis, they loaded relatively weakly on both gradients compared to cortical regions. We suspect that this reflects relatively stronger cortico-cortico functional connectivity (compared to cortico-extracortico connectivity), rather than the non-involvement of these regions in learning. As cortico-cerebellar/striatal functional connectivity is relatively weaker, and so noisier, it may simply be less predictively useful than cortico-cortical connectivity. Thus, our results should not be taken to suggest that, for example, cerebellar circuitry does not play a fundamental role in implicit learning processes.

3 Methods

3.1 Participants

Forty-six right-handed subjects (27 females, aged 18-28 years, mean age: 20.3 years) participated in three separate testing sessions, each spaced approximately 1 week apart: the first, an MRI-training session, was followed by two subsequent MRI experimental sessions. Of these 46 subjects, 10 participants were excluded from the final analysis [1 subject was excluded due of excessive head motion in the MRI scanner (motion greater than 2 mm or 2° rotation within a single scan); 1 subject was excluded due interruption of the scan during the learning phase of the RL task; 5 subjects were excluded due to poor behavioural performance in one or both tasks (4 of these participants were excluded because >25% of trials were not completed within the maximum trial duration; and one because >20% of trials had missing data due to insufficient pressure of the fingertip on the MRI-compatible tablet); 3 subjects were excluded due to a failure to properly perform the RL task (these subjects did not trace the visible rightward path during the baseline phase, but rather continued to trace a straight line for the entire duration of the task, suggesting that they did not attend to the task)]. Right-handedness was assessed with the Edinburgh handedness questionnaire (Oldfield, 1971). Participants' informed consent was obtained before beginning the experimental protocol. The Queen's University Research Ethics Board approved the study and it was conducted in coherence to the principles outlines in the Canadian Tri-Council Policy Statement on Ethical Conduct for Research Involving Humans and the principles of the Deceleration of Helsinki (1964).

3.2 Procedure

In the first session, participants took part in an MRI-training session inside a mock (0 T) scanner, that was made to look and sound like a real MRI scanner. We undertook this training session to (1) introduce participants to features of the EL and RL tasks that would be subsequently performed in the MRI scanner, (2) ensure that subjects obtained baseline performance levels on those two tasks, and (3) ensure that participants could remain still for 1 hr. To equate baseline performance levels across participants, subjects performed 80 trials per task. To train participants to remain still in the scanner, we monitored subjects' head movement via a Polhemus sensor attached to each subject's forehead (Polhemus, Colchester, Vermont). This allowed a real-time read-out of subject head displacement in the three axes of translation and rotation (6 dimensions total). Whenever subjects' head translation and/or rotation reached 0.5 mm or 0.5º rotation, subjects received an unpleasant auditory tone, delivered through a speaker system located near the head. All of the subjects used in the study learned to constrain their head movement through this training regimen. Following this first session, subjects then subsequently participated in RL and EL tasks, respectively (see below for details).

3.3 Apparatus

During testing in the mock (0 T) scanner, subjects performed hand movements that were directed towards a target by applying finger tip pressure on a digitizing touchscreen tablet (Wacom Intuos Pro M tablet). During the actual MRI

testing sessions, subjects used an MRI-compatible digitizing tablet (Hybridmojo LLC, CA, USA). In both the mock and real MRI scanner, the target and cursor stimuli were rear-projected with an LCD projector (NEC LT265 DLP projector, 1024 x 768 resolution, 60 Hz refresh rate) onto a screen mounted behind the participant. The stimuli on the screen were viewed through a mirror fixated on the MRI coil directly above the participants' eyes, thus preventing the participant from being able to see their hand.

3.4 Reward-based Learning (RL) task

In the RL task (Figure 1, top right), participants learned to produce, through reward-based feedback, finger movement trajectories with a specific (unseen) shape. Specifically, subjects were instructed to repeatedly trace, without visual cursor feedback of their actual finger paths, a subtly curved path displayed on the screen (the visible path). During learning trials, participants were told that, following each trial, they would receive a score based on how accurately they traced the visible path (and were instructed to maximize points across trials). However, unbeknownst to them, they actually received points based on how well they traced the mirror-image path (the target path). Critically, because participants received no visual feedback about their actual finger trajectories or the 'rewarded' shape, they could not use error-based information to guide learning. Our task was inspired by the motor learning tasks developed by (Wu et al., 2014).

Each trial started with the participant moving the cursor (3 mm radius cyan circle) into the start position (4 mm radius white circle) at the bottom of the screen by sliding their index finger on the tablet. The cursor was only visible when it was within 30 mm of the start position. After the cursor was held within the start position for 0.5 s, the cursor disappeared and a curved path and a target distance marker appeared on the screen. The target distance marker was a horizontal red line (30 x 1 mm) that appeared 60 mm above the start position. The visible path connected the start position and target distance marker and had the shape of a half sine wave with an amplitude of 0.15 times the target distance. Participants were instructed to trace the curved visible path. When the cursor reached the target marker distance, the marker changed colour from red to green to indicate that the trial was completed. Importantly, participants did not receive feedback about the position of their cursor during the trial.

In the baseline block, participants did not receive feedback about their performance. In the learning block, participants were rewarded 0 to 100 points after reaching the target distance marker, and participants were instructed to do their best to maximize this score (the points were displayed as text centrally on the screen). They were told that to increase the score, they had to trace the line more accurately. Each trial was terminated after 4.5 s, independent of whether the cursor had reached the target. After a delay of 1.5 s, allowing time to save the data, the next trial started with the presentation of the start position.

To calculate the score on each trial in the learning block, the x position of the cursor was interpolated at each cm displacement from the start position in the y direction (i.e., at exactly 10, 20, 30, 40, 50 and 60 mm). For each of the six y positions, the absolute distance between the interpolated x position of the cursor and the x position of the rewarded path (mirror image of visible path) was calculated. The sum of these errors was scaled by dividing it by the sum of

errors obtained for a half cycle sine-shaped path with an amplitude of 0.5 times the target distance, and then multiplied by 100 to obtain a score ranging between 0 and 100. The scaling worked out so that a perfectly traced visible path would result in an imperfect score of 40 points. This scaling was chosen on the basis of extensive pilot testing in order to achieve variation in subject performance, and to ensure that subjects still received informative score feedback when tracing in the vicinity of the visible trajectory.

During the participant training session in the mock MRI scanner (i.e., 1-week prior to the MRI testing session), participants only performed a practice block in which they traced a straight line with (40 trials) and then without (40 trials) visual feedback of the position of the cursor during the reach. This training session exposed participants to several key features of the task (e.g., use of the touchscreen tablet, trial timing, presence and removal of cursor feedback), allowed us to establish adequate performance levels, but importantly did not allow for any reward-based learning to take place.

At the beginning of the MRI testing session, but prior to the first scan being collected, participants re-acquainted themselves with the RL task by first performing a practice block in which they traced a straight line with (40 trials) and then without (40 trials) visual feedback of the position of the cursor during the reach. Next, we collected an anatomical scan, following by a DTI scan, followed by a resting-state fMRI scan. During the latter resting-state scans, participants were instructed to rest with their eyes open while fixating on a central cross location presented on the screen. Following this, participants performed the RL task, which consisted of two separate experimental runs without visual feedback of the cursor: (1) a baseline block of 70 trials in which they attempted to trace the curved visible path and no score was provided, and (2) a separate learning block of 200 trials in which participants were instructed to maximize their score shown at the end of each trial.

3.5 Error-based Learning (EL) task

To study EL, we used the well-characterized visuomotor rotation (VMR) paradigm (Krakauer, 2009, ; Figure 1, top left). During the VMR task, participants performed baseline trials in which they used their right index finger to perform center-out target-directed movements. After these baseline trials, we applied a $45°$ clockwise (CW) rotation to the viewed cursor, allowing investigation of VMR learning. Following this, we assessed participants' re-aiming strategy associated with their learning.

Each trial started with the participant moving the cursor (3 mm radius cyan circle) into the start position (4 mm radius white circle) in the centre of the screen by sliding the index finger on the tablet. To guide the cursor to the start position, a ring centred around the start position indicated the distance between the cursor and the start position. The cursor became visible when its centre was within 8 mm of the centre of the start position. After the cursor was held within the start position for 0.5 s, a target (5 mm radius red circle) was shown on top of a grey ring with a radius of 60 mm (i.e., the target distance) centred around the start position. The target was presented at one of eight locations, separated by $45°$ (0, 45, 90, 135, 180, 225, 270 and 315°), in randomized bins of eight trials. Participants were instructed to hit the target with the cursor by making a fast finger movement on the tablet. They were instructed to 'slice' the cursor through

the target to minimize online corrections during the reach. If the movement was initiated (i.e., the cursor had moved fully out of the start circle) before the target appeared, the trial was aborted and a feedback text message "Too early" appeared centrally on the screen. In trials with correct timing, the cursor was visible during the movement to the ring and then became stationary for one second when it reached the ring, providing the participant with visual feedback of their endpoint reach error. If any part of the stationary cursor overlapped with any part of the target, the target coloured green to indicate a hit. Each trial was terminated after 4.5 s, independent of whether the cursor had reached the target. After a delay of 1.5 s, allowing time to save the data, the next trial started with the presentation of the start position.

During the participant training session in the mock MRI scanner (i.e., 2-weeks prior to the VMR MRI testing session), participants performed a practice block of 40 trials with veridical feedback (i.e., no rotation was applied to the cursor). As with the RL task, this training session exposed participants to several key features of the task (e.g., use of the touchscreen tablet, trial timing, used of cursor feedback to correct for errors) and allowed us to establish adequate performance levels.

At the beginning of the MRI testing session, but prior to the first scan being collected, participants re-acquainted themselves with the EL task by performing 80 practice trials with veridical cursor feedback. Next, we collected an anatomical scan, followed by the baseline fMRI experimental run, wherein subjects performed 64 trials of the EL task with veridical cursor feedback using their right hand. Next, they performed the learning scan, wherein subjects performed 160 trials in which feedback of the cursor during the reach was rotated clockwise by $45°$. Following this fMRI experimental run, participants were asked to report their strategic aiming direction (over 16 trials). In these trials, a line between the start and target position appeared on the screen at the start of each trial. Participants were asked to use a separate MRI joystick (Current Designs, Inc.) positioned at their left hip to rotate the line to the direction that they would aim their finger movement in for the cursor to hit the target, and click the button on the joystick box when satisfied. Following the button click, the trial proceeded as a normal reach trial. These 16 "report" trials were followed by 16 normal rotation trials. As several subjects expressed confusion about the nature of the report trials, often failing to adjust the line at all during the first few trials, we discarded the first 8 report trials for all subjects, and calculated the mean aim direction using the final 8 trials. Note that we had subjects perform these report trials following learning (as in de Brouwer et al., 2022) given our prior behavioural work showing that the inter-mixing of report trials during learning can lead to more participants adopting an explicit, re-aiming strategy (de Brouwer et al., 2018, 2022), thereby distorting participants' learning curves. Participants were not informed about nature or presence of the visuomotor rotation before or during the experiment.

Note that all subjects performed the EL task during the second testing session (i.e., testing order was not counterbalanced across the RL and EL tasks). We made this decision in light of our knowledge that subjects alter their behavior after performing explicit report trials in the EL task (de Brouwer et al., 2018) (i.e., often developing explicit awareness of the perturbation and using that to guide their performance). We were concerned that, had subjects performed the EL task first, they may have anticipated some experimental manipulation (or deception), and thus would not have approached the RL task in a naive fashion. From this perspective, our approach of having defined the explicit and implicit learning

gradients on the (second) EL task and then using those gradients to predict performance on the (first) RL task (as done in the main manuscript), strengthens our interpretations of the effects.

3.6 Behavioral data analysis

3.6.1 EL task analysis

Trials in which the reach was initiated before the target appeared (4% of trials) or in which the cursor did not reach the target within the time limit (5% of trials) were excluded from the offline analysis of hand movements. As insufficient pressure on the touchpad resulted in a default state in which the cursor was reported as lying in the top left corner of the screen, we also excluded trials in which the cursor jumped to this position before reaching the target region (2% of trials). We then applied a conservative threshold on the movement and reaction times, removing the top $.05\%$ of trials across all subjects. As the EL task required the subject to determine the target location prior to responding, we also set a lower threshold of 100 ms on the reaction time.

We then calculated the angle difference between the target position and the last sample before the cursor exceeded the target circle. This was then converted to an adaptation score by subtracting the angle of the rotation on each trial ($0°$ during baseline, and $45°$ during learning) in order to derive the actual aim direction on each trial. For consistency with the RL task, we flipped the sign of this score so that positive values always reflected better performance.

3.6.2 RL task analysis

Trials in which the cursor did not reach the target distance marker within the time limit were excluded from the offline analysis of hand movements (1% of trials). As in the EL task, we excluded trials in which insufficient pressure was applied (2% of trials), and also separately applied a conservative threshold on the movement and reaction times, removing the top $.05\%$ of trials across all subjects. As the RL task did not involve response discrimination, we did not set a lower threshold on these variables.

3.6.3 Functional PCA of subject behavioral data

All subject behavioral data were averaged over 8 trial bins. In the EL task, this corresponded to the natural binned structure of the task, with one presentation of each of the 8 target locations. For consistency between tasks, we used an identical window size for the RL task (creating 40 8-trial bins during learning). We represented individual learning curves as functional data using a cubic spline basis with a smoothing penalty estimated by generalized cross-validation (Härdle, 1990). For the analysis of each task, we separately performed functional PCA (Shang, 2014) in order to extract components capturing the dominant patterns of variability in subject-level performance. In both tasks, the top component described overall learning, and explained a majority of the variability (75%) in performance. Spline smoothing and fPCA were performed using the R package fda (Ramsay et al., 2022), and example code is provided in a publicly available repository (see Data and Code Availability statement).

3.6.4 Bayesian multivariate regression model

Our model of subjects' joint performance in the EL and RL tasks (see Figure 3) is essentially a bivariate linear regression model with correlated errors, allowing subjects' reported aim direction in the EL task to affect both the mean performance in each task, as well as the error correlation. The effect of subjects' explicit report is assumed to be linear on the scale of the Fisher transformed correlation.

Let $\mathbf{y}_{\text{EL}}$ and $\mathbf{y}_{\text{RL}}$ be vectors of subjects' EL and RL component scores, respectively, and let $\mathbf{x}_{\text{Rep}}$ be subjects mean reported aim direction during the EL report block. We fit a multivariate regression model

$$\mathbf{Y} = \mathbf{X}\mathbf{B} + \mathbf{E} \tag{1}$$

where $\mathbf{Y} = [\mathbf{y}_{\text{EL}}\ \mathbf{y}_{\text{RL}}]$ and $\mathbf{X} = [\mathbf{1}\ \mathbf{x}_{\text{Rep}}]$ is the design matrix. We assume that the errors $\epsilon_i = [\epsilon_{\text{EL}_i}\ \epsilon_{\text{RL}_i}]$ are independent and jointly normal, with covariance

$$\Sigma_i = \begin{bmatrix} \sigma^2 & \sigma^2 r_i \\ \sigma^2 r_i & \sigma^2_{\text{RL}} \end{bmatrix}, \tag{2}$$

where r_i is the correlation between $\mathbf{e}_{\text{EL}_i}$ and $\mathbf{e}_{\text{RL}_i}$. The Fisher transform of r_i is allowed to vary as a linear function of $\mathbf{x}_{\text{Rep}}$, so that

$$\text{artanh}(r_i) = \alpha_{\text{r}} + \beta_{\text{r}} x_{\text{Rep}_i}. \tag{3}$$

We place weakly informative standard normal priors over the coefficients, and half-Cauchy priors over the covariance parameters $(\sigma^2_{\text{EL}}, \sigma^2_{\text{RL}})$. The full model is thus

$$\begin{aligned}
\mathbf{Y} &= \mathbf{X}\mathbf{B} + \mathbf{E} \\
\mathbf{B} &= \begin{bmatrix} \alpha_{\text{EL}} & \alpha_{\text{RL}} \\ \beta_{\text{EL}} & \beta_{\text{RL}} \end{bmatrix} \\
\mathbf{e}_i &\sim \text{MVN}(\mathbf{0}, \Sigma_i) \\
\Sigma_i &= \begin{bmatrix} \sigma & 0 \\ 0 & \sigma \end{bmatrix} \begin{bmatrix} 1 & r \\ r & 1 \end{bmatrix} \begin{bmatrix} \sigma & 0 \\ 0 & \sigma \end{bmatrix} \\
\text{arctanh}(r) &= \alpha_{\text{r}} + \beta_{\text{r}} x_{\text{Rep}_i} \\
\sigma_{\text{EL}}, \sigma_{\text{RL}} &\sim \text{Cauchy}^{+}(0, 1) \\
\alpha_{\text{r}}, \beta_{\text{r}} &\sim \text{N}(0, 1)
\end{aligned} \tag{4}$$

The model was fit by Hamiltonian Monte-Carlo in RStan (Stan Development Team, 2022) using 4 chains of 4000 samples, of which the first 1000 were discarded as burn-in. Chains were inspected visually, and for all parameters we observed $\hat{R} < 1.01$.

To visualize the model predictions, we used the posterior mean parameters estimates. For a given explicit report x_{Rep_i}, the predicted distribution of EL and RL scores is then

$$\begin{aligned} \begin{bmatrix} y_{\text{EL}} \\ y_{\text{RL}} \end{bmatrix}_i &\sim \text{MVN}\left(\begin{bmatrix} \hat{\alpha}_{\text{EL}} + \hat{\beta}_{\text{EL}} x_{\text{Rep}_i} \\ \hat{\alpha}_{\text{RL}} + \hat{\beta}_{\text{RL}} x_{\text{Rep}_i} \end{bmatrix}, \begin{bmatrix} \hat{\sigma}^2 & \hat{\sigma}^2 r_i \\ \hat{\sigma}^2 r_i & \hat{\sigma}^2 \end{bmatrix} \right) \\ r_i &= \hat{\alpha}_{\text{r}} + \hat{\beta}_{\text{r}} x_{\text{Rep}_i} \end{aligned} \tag{5}$$

Where hats denote posterior mean estimates. The predictions are illustrated in Figure 3 (bottom right) as confidence ellipses representing a Mahalanobis distance of 1 from the mean.

3.7 MRI Acquisition

Participants were scanned using a 3-Tesla Siemens TIM MAGNETOM Trio MRI scanner located at the Centre for Neuroscience Studies, Queen's University (Kingston, Ontario, Canada). Functional MRI volumes were acquired using a 32-channel head coil and a T2*-weighted single-shot gradient-echo echo-planar imaging (EPI) acquisition sequence (time to repetition (TR) = 2000 ms, slice thickness = 4 mm, in-plane resolution = 3 mm x 3 mm, time to echo (TE) = 30 ms, field of view = 240 mm x 240 mm, matrix size = 80 x 80, flip angle = 90°, and acceleration factor (integrated parallel acquisition technologies, iPAT) = 2 with generalized auto-calibrating partially parallel acquisitions (GRAPPA) reconstruction. Each volume comprised 34 contiguous (no gap) oblique slices acquired at a 30° caudal tilt with respect to the plane of the anterior and posterior commissure (AC-PC), providing whole-brain coverage of the cerebrum and cerebellum. Each of the task-related scans included an additional 8 imaging volumes at both the beginning and end of the scan. On average, each of the MRI testing sessions lasted 2 hrs.

At the beginning of the RL MRI testing session, a T1-weighted ADNI MPRAGE anatomical was also collected (TR = 1760 ms, TE = 2.98 ms, field of view = 192 mm x 240 mm x 256 mm, matrix size = 192 x 240 x 256, flip angle = 9°, 1 mm isotropic voxels). This was followed by a series of Diffusion-Weighted scans, wherein we acquired two sets of whole-brain diffusion-weighted volumes (30 directions, b = 1000 s mm-2, 65 slices, voxel size = 2 x 2 x 2 mm3, TR = 9.3 s, TE = 94 ms) plus 2 volumes without diffusion-weighting (b = 0 s mm-2). Next, we collected a resting-state scan, wherein 300 imaging volumes were acquired. For the baseline and learning scans during RL testing, 222 and 612 imaging volumes were acquired, respectively.

At the beginning of the EL MRI testing session, we gathered high-resolution whole-brain T1-weighted (T1w) and T2-weighted (T2w) anatomical images (in-plane resolution 0.7 x 0.7 mm2; 320 x 320 matrix; slice thickness: 0.7 mm; 256 AC-PC transverse slices; anterior-to-posterior encoding; 2 x acceleration factor; T1w TR 2400 ms; TE 2.13 ms;

flip angle 8º; echo spacing 6.5 ms; T2w TR 3200 ms; TE 567 ms; variable flip angle; echo spacing 3.74 ms). These protocols were selected on the basis of protocol optimizations designed by Filippini et al. (2014). Following this, for the baseline and learning functional scans, 204 and 492 imaging volumes were acquired, respectively.

3.8 fMRI Preprocessing

Results included in this manuscript come from preprocessing performed using *fMRIPrep* 1.4.1 (Esteban et al. (2018b); Esteban et al. (2018a); RRID:SCR_016216), which is based on *Nipype* 1.2.0 (Gorgolewski et al. (2011); Gorgolewski et al. (2018); RRID:SCR_002502).

Anatomical data preprocessing A total of 2 T1-weighted (T1w) images were found within the input BIDS dataset. All of them were corrected for intensity non-uniformity (INU) with `N4BiasFieldCorrection` (Tustison et al., 2010), distributed with ANTs 2.2.0 (Avants et al., 2008, RRID:SCR_004757). The T1w-reference was then skull-stripped with a *Nipype* implementation of the `antsBrainExtraction.sh` workflow (from ANTs), using OASIS30ANTs as target template. Brain tissue segmentation of cerebrospinal fluid (CSF), white-matter (WM) and gray-matter (GM) was performed on the brain-extracted T1w using `fast` (FSL 5.0.9, RRID:SCR_002823, Zhang et al., 2001). A T1w-reference map was computed after registration of 2 T1w images (after INU-correction) using `mri_robust_template` (FreeSurfer 6.0.1, Reuter et al., 2010). Brain surfaces were reconstructed using `recon-all` (FreeSurfer 6.0.1, RRID:SCR_001847, Dale et al., 1999), and the brain mask estimated previously was refined with a custom variation of the method to reconcile ANTs-derived and FreeSurfer-derived segmentations of the cortical gray-matter of Mindboggle (RRID:SCR_002438, Klein et al., 2017). Volume-based spatial normalization to two standard spaces (MNI152NLin6Asym, MNI152NLin2009cAsym) was performed through nonlinear registration with `antsRegistration` (ANTs 2.2.0), using brain-extracted versions of both T1w reference and the T1w template. The following templates were selected for spatial normalization: *FSL's MNI ICBM 152 non-linear 6th Generation Asymmetric Average Brain Stereotaxic Registration Model* [Evans et al. (2012), RRID:SCR_002823; TemplateFlow ID: MNI152NLin6Asym], *ICBM 152 Nonlinear Asymmetrical template version 2009c* [Fonov et al. (2009), RRID:SCR_008796; TemplateFlow ID: MNI152NLin2009cAsym].

Functional data preprocessing For each of the BOLD runs per subject (across all tasks and sessions), the following preprocessing was performed. First, a reference volume and its skull-stripped version were generated using a custom methodology of *fMRIPrep*. The BOLD reference was then co-registered to the T1w reference using `bbregister` (FreeSurfer) which implements boundary-based registration (Greve and Fischl, 2009). Co-registration was configured with nine degrees of freedom to account for distortions remaining in the BOLD reference. Head-motion parameters with respect to the BOLD reference (transformation matrices, and six corresponding rotation and translation parameters) are estimated before any spatiotemporal filtering using `mcflirt` (FSL 5.0.9, Jenkinson et al., 2002). BOLD runs were slice-time corrected using `3dTshift` from AFNI 20160207 (Cox and Hyde, 1997, RRID:SCR_005927). The BOLD time-series, were resampled to

surfaces on the following spaces: *fsaverage*. The BOLD time-series (including slice-timing correction when applied) were resampled onto their original, native space by applying a single, composite transform to correct for head-motion and susceptibility distortions. These resampled BOLD time-series will be referred to as *preprocessed BOLD in original space*, or just *preprocessed BOLD*. The BOLD time-series were resampled into several standard spaces, correspondingly generating the following *spatially-normalized, preprocessed BOLD runs*: MNI152NLin6Asym, MNI152NLin2009cAsym. First, a reference volume and its skull-stripped version were generated using a custom methodology of *fMRIPrep*. Automatic removal of motion artifacts using independent component analysis (ICA-AROMA, Pruim et al., 2015) was performed on the *preprocessed BOLD on MNI space* time-series after removal of non-steady state volumes and spatial smoothing with an isotropic, Gaussian kernel of 6mm FWHM (full-width half-maximum). Corresponding "non-aggresively" denoised runs were produced after such smoothing. Additionally, the "aggressive" noise-regressors were collected and placed in the corresponding confounds file. Several confounding time-series were calculated based on the *preprocessed BOLD*: framewise displacement (FD), DVARS and three region-wise global signals. FD and DVARS are calculated for each functional run, both using their implementations in *Nipype* (following the definitions by Power et al., 2014). The three global signals are extracted within the CSF, the WM, and the whole-brain masks. Additionally, a set of physiological regressors were extracted to allow for component-based noise correction (*CompCor*, Behzadi et al., 2007). Principal components are estimated after high-pass filtering the *preprocessed BOLD* time-series (using a discrete cosine filter with 128s cut-off) for the two *CompCor* variants: temporal (tCompCor) and anatomical (aCompCor). tCompCor components are then calculated from the top 5% variable voxels within a mask covering the subcortical regions. This subcortical mask is obtained by heavily eroding the brain mask, which ensures it does not include cortical GM regions. For aCompCor, components are calculated within the intersection of the aforementioned mask and the union of CSF and WM masks calculated in T1w space, after their projection to the native space of each functional run (using the inverse BOLD-to-T1w transformation). Components are also calculated separately within the WM and CSF masks. For each CompCor decomposition, the k components with the largest singular values are retained, such that the retained components' time series are sufficient to explain 50 percent of variance across the nuisance mask (CSF, WM, combined, or temporal). The remaining components are dropped from consideration. The head-motion estimates calculated in the correction step were also placed within the corresponding confounds file. The confound time series derived from head motion estimates and global signals were expanded with the inclusion of temporal derivatives and quadratic terms for each (Satterthwaite et al., 2013). Frames that exceeded a threshold of 0.5 mm FD or 1.5 standardised DVARS were annotated as motion outliers. All resamplings can be performed with *a single interpolation step* by composing all the pertinent transformations (i.e. head-motion transform matrices, susceptibility distortion correction when available, and co-registrations to anatomical and output spaces). Gridded (volumetric) resamplings were performed using `antsApplyTransforms` (ANTs), configured with Lanczos interpolation to minimize the smoothing effects of other kernels (Lanczos, 1964). Non-gridded (surface) resamplings were performed using `mri_vol2surf` (FreeSurfer).

Many internal operations of *fMRIPrep* use *Nilearn* 0.5.2 (Abraham et al., 2014, RRID:SCR_001362), mostly within the functional processing workflow. For more details of the pipeline, see the section corresponding to workflows in *fMRIPrep*'s documentation.

3.8.1 ROI extraction

Regions of interest were identified using separate parcellations for the cerebellum, basal ganglia, and cortex. For the cerebellum, we extracted all regions using the atlas of Diedrichsen (Diedrichsen, 2006); For the basal ganglia, we extracted the caudate, putamen, accumbens, and pallidum, using the Harvard Oxford atlas (Frazier et al., 2005; Makris et al., 2006). Finally, for cortex, we extracted regions using the 400 region Schaefer parcellation (Schaefer et al., 2018). For the Somatomotor A and B networks, we extracted only those regions which Schaefer et al. identified as being activated during finger and tongue movement. For all regions and networks, we created timeseries data by computing the mean BOLD signal within each ROI.

3.8.2 Covariance estimation and centering

For each subject, we used the Ledoit and Wolf shrinkage estimator (Ledoit and Wolf, 2004) to derive covariance matrices for periods of equivalent length (100 imaging volumes) during baseline, and the beginning and end of the learning blocks of each task. For the the baseline blocks, we extracted 100 imaging volumes equally spaced throughout the scan, so as the capture the entirety of the baseline epoch of the task.

To center the covariance matrices, we took the approach advocated by Zhao et al. (2018), which leverages the natural geometry of the space of covariance matrices. We have implemented many of the computations required to replicate the analysis in an publicly available R package **spdm**, which is freely available from a Git repository at https://github.com/areshenk-rpackages/spdm.

The procedure is as follows. Letting S_{ij} denote the j'th covariance matrix for subject i, we computed the grand mean covariance $\bar{S}$ over all subjects using the fixed-point algorithm described by Congedo et al. (2017), as well as subject means $\bar{S}_i$. We then projected the each covariance matrix S_{ij} onto the tangent space at $\bar{S}_i$ to obtain a tangent vector

$$T_{ij} = \bar{S}_i^{1/2} \log(\bar{S}_i^{-1/2} S_{ij} \bar{S}_i^{-1/2}) \bar{S}_i^{1/2}, \tag{6}$$

where $\log$ denotes the matrix logarithm. The tangent vector T_{ij} then encodes the *difference* in covariance between the covariance S_{ij} and the subject mean $\bar{S}_i$. We then transported each tangent vector to the grand mean $\bar{S}$ using the transport proposed by Zhao et al. (2018), obtaining a centered tangent vector T_{ij}^c given by

$$T_{ij}^c = G T_{ij} G^\top \tag{7}$$

where $G = \bar{S}^{1/2} \bar{S}_i^{-1/2}$. This centered tangent vector (a symmetric matrix) encodes the same difference in covariance, but now expressed relative to the mean resting state scan.

3.8.3 Construction of the Explicit and Implicit Learning Gradients and Prediction of RL performance

Here we describe our approach for the main analysis – i.e., construction of the (performance corrected) explicit gradient derived from the contralateral hand area, during the early learning epoch.

For each tangent vector in the early learning epoch, we computed the mean connectivity between the contralateral hand area (within the somatomotor network) and the remaining ROIs. The resulting vectors (containing an entry for each non-motor ROI) were used as the features for our predictive model. Call the resulting matrix of predictors $\mathbf{X} = [\mathbf{x_1}, \mathbf{x_2}, \ldots, \mathbf{x_n}]$, where $\mathbf{x_i}$ is a vector containing the mean connectivity of the i'th ROI with the hand area of motor cortex. We then computed the explicit learning score for each subject, defined as the circular mean difference between the target location and the subject's reported aim direction. These scores formed the response variable $\mathbf{y}$. Our *corrected* scores were then derived by orthogonalizing with respect to subjects' EL task scores. That is, we regressed $\mathbf{y}$ onto the vector of EL task scores and used the residuals for our analysis, and the same was done for each predictor (that is, each column in $\mathbf{X}$). Both the predictors and outcome were then standardized prior to analysis.

We then fit a ridge regression model with separate network-level penalty terms using the model described by (Van De Wiel et al., 2016), and implemented in the R package `GRridge` (van de Wiel and Novianti, 2022). That is, each of the 17 networks comprising the predictors – 15 non-motor cortical networks, plus cerebellum and basal ganglia – possessed their own shrinkage parameters. These parameters were separately tuned using an internal leave-one-out cross-validation loop, so that networks whose regions contributed relatively little to overall predictive performance were shrunken more harshly relative to predictively useful networks. The precise arguments were as follows:

```
grridge(X, y, partitions = network_labels,
        unpenal = ~1, offset = NULL, method = "stable",
        niter = 10, innfold = NULL, fixedfoldsinn = TRUE,
        selectionEN = F, cvlmarg = 1, savepredobj = "all")
```

The resulting parameter vector $\boldsymbol{\beta}$ contains, for each ROI, its estimated conditional contribution to subjects' explicit report. We then derived, for each subject, the mean functional connectivity of each region with the motor cortex during the early learning epoch of the RL task (derived from the centered tangent vectors, as described above). The Pearson correlation between this vector and the vector $\boldsymbol{\beta}$ was the subject's *explicit gradient score*.

Note that all other models (such as the derivation of the implicit gradient, or gradients using separate areas of motor cortex or different time windows, such as baseline or late learning) were constructed identically, *mutatis mutandis* (e.g. using implicit scores rather than explicit reports).

3.8.4 Gradient embedding

All brain maps used for comparison with our explicit alignment gradient were processed using the Python package `Neuromaps` (Markello et al., 2022). Table 1 includes a complete list of these gradients, along with their identifying keywords. All gradients were converted into fsLR space and re-sampled to 32k vertices.

For each brain map, we generated 1000 spatial null maps using the procedure outlined by Cornblath et al. (2020): Roughly, each brain map was projected to a sphere, and then projected back onto the cortical surface after a random rotation. Each permuted (spatial null) map was then parcellated according to Schaefer et al. (2018), taking the mean value within each parcel. We then computed the Pearson correlation between these null maps and our explicit alignment gradient in order to derive the null distributions displayed in Figure 7. Note that one brain map – the developmental expansion gradient (Hill et al., 2010) – has data provided only for the right hemisphere, and so it was mirrored symmetrically onto the left hemisphere. Though imperfect, we believe this is a reasonable approximation, as the results reported by Hill et al. are highly symmetric.

Given two brain maps represented as a vector x and y of ROIs, we defined the distance between the two to be the angle between the subspaces spanned by each vector (that is, the principal angle between them). In the one-dimensional case, this is equivalent to |acos(r)|, where r is the Pearson correlation when x and y are centered. We chose this distance measure, rather than one based on the correlation itself, because several brain maps used in our analysis were derived from principal component analysis (or other such embeddings), and thus the sign of the gradients was arbitrary. Thus, in order to avoid an embedding which separated two spatially similar brain maps (e.g., the Margulies gradient 1 and the myelin concentration map; Huntenburg et al., 2017) merely due to a difference in sign, we chose a metric which encoded the direction of the gradient (e.g. anterior-posterior, dorsal-ventral) rather than the positive or negative end of the gradient itself. We then visualized these gradients using a two-dimensional spherical projection (De Leeuw and Mair, 2009, ; Figure 7, bottom). A spherical – as opposed to Euclidean – projection was chosen due to the fact that, under our distance measure, gradients travelling in opposite directions necessarily "wrap around" after sufficient distance. For example, starting at an anterior-posterior gradient and rotating it clockwise vs. counter-clockwise will produce two diverging gradients which eventually coincide at a dorsal-ventral gradient.

	source	**desc**	**note**
Margulies gradient 1	margulies2016	fcgradient01	Sign flipped
Cognitive PC1	neurosynth	cogpc1	Sign flipped
Cohomology	xu2020	FChomology	
Intersubject variability	mueller2013	intersubjvar	
Opioid	turtonen2020	carfentanil	
DA1	kaller2017	sch23390	
DA2	smith2017	flb457	
Glutamate	rosaneto	abp688	
5-HT	savli2012	p943	
Norepinephrine	hesse2017	methylreboxetine	
Acetylcholine	naganawa2020	lsn3172176	
Alpha	hcps1200	megalpha	
Beta	hcps1200	megbeta	
Gamma (low)	hcps1200	meggamma1	
Gamma (high)	hcps1200	meggamma2	
Delta	hcps1200	megdelta	
Theta	hcps1200	megtheta	
Intrinsic timescale	hcps1200	megtimescale	
Genetic PC1	abagen	genepc1	Sign flipped
Developmental expansion	hill2010	devexp	Mirrored to left hem.
Relative scaling	reardon2018	scalinghcp	
Evolutionary expansion	xu2020	evoexp	
Myelin	hcps1200	myelinmap	

Table 1: Gradients used for analysis. Keywords **source** and **desc** denote neuromaps annotations.

Acknowledegments

C.N.A. was supported by a Natural Sciences and Engineering Research Council (NSERC) graduate award. J.P.G. was also supported by a NSERC Discovery Grant (RGPIN-2017-04684), Canadian Institutes of Health Research Grant (MOP126158), and Botterell Foundation Award, as well as funding from the Canadian Foundation for Innovation (35559). The authors would like to thank Martin York and Sean Hickman for technical assistance, and thank Don O'Brien for assistance with data collection.

Data availability

Behavioral and imaging data are archived at Queens University and are available from the authors upon reasonable request.

Code availability

Imaging data were preprocessed using fmriPrep 1.4.0, which is open source and freely available. Operations on covariance matrices, including estimation and centering, were performed using the R package spdm, which is freely available in a repository at `https://github.com/areshenk-rpackages/spdm`. Tutorial code and data for implementing the centering procedure and gradient analyses are hosted in a GitHub repository at `https://github.com/areshenk-opendata/2023-implicitexplicit`.

References

Abraham, A., Pedregosa, F., Eickenberg, M., Gervais, P., Mueller, A., Kossaifi, J., Gramfort, A., Thirion, B., and Varoquaux, G. (2014). Machine learning for neuroimaging with scikit-learn. *Frontiers in Neuroinformatics*, 8.

Andrews-Hanna, J. R., Reidler, J. S., Sepulcre, J., Poulin, R., and Buckner, R. L. (2010). Functional-anatomic fractionation of the brain's default network. *Neuron*, 65(4):550–562.

Anguera, J. A., Reuter-Lorenz, P. A., Willingham, D. T., and Seidler, R. D. (2010). Contributions of spatial working memory to visuomotor learning. *Journal of cognitive neuroscience*, 22(9):1917–1930.

Areshenkoff, C., Gale, D. J., Standage, D., Nashed, J. Y., Flanagan, J. R., and Gallivan, J. P. (2022). Neural excursions from manifold structure explain patterns of learning during human sensorimotor adaptation. *Elife*, 11:e74591.

Avants, B., Epstein, C., Grossman, M., and Gee, J. (2008). Symmetric diffeomorphic image registration with cross-correlation: Evaluating automated labeling of elderly and neurodegenerative brain. *Medical Image Analysis*, 12(1):26–41.

Baldassano, C., Chen, J., Zadbood, A., Pillow, J. W., Hasson, U., and Norman, K. A. (2017). Discovering event structure in continuous narrative perception and memory. *Neuron*, 95(3):709–721.

Behzadi, Y., Restom, K., Liau, J., and Liu, T. T. (2007). A component based noise correction method (CompCor) for BOLD and perfusion based fmri. *NeuroImage*, 37(1):90–101.

Binder, J. R., Desai, R. H., Graves, W. W., and Conant, L. L. (2009). Where is the semantic system? a critical review and meta-analysis of 120 functional neuroimaging studies. *Cerebral cortex*, 19(12):2767–2796.

Bond, K. M. and Taylor, J. A. (2015). Flexible explicit but rigid implicit learning in a visuomotor adaptation task. *Journal of neurophysiology*, 113(10):3836–3849.

Braitenberg, V. (1962). A note on myeloarchitectonics. *Journal of comparative Neurology*, 118(2):141–156.

Buckner, R. L. and Krienen, F. M. (2013). The evolution of distributed association networks in the human brain. *Trends in cognitive sciences*, 17(12):648–665.

Christou, A. I., Miall, R. C., McNab, F., and Galea, J. M. (2016). Individual differences in explicit and implicit visuomotor learning and working memory capacity. *Scientific reports*, 6(1):1–13.

Codol, O., Holland, P. J., and Galea, J. M. (2018). The relationship between reinforcement and explicit control during visuomotor adaptation. *Scientific reports*, 8(1):1–11.

Cole, S. R., Platt, R. W., Schisterman, E. F., Chu, H., Westreich, D., Richardson, D., and Poole, C. (2010). Illustrating bias due to conditioning on a collider. *International journal of epidemiology*, 39(2):417–420.

Congedo, M., Barachant, A., and Koopaei, E. K. (2017). Fixed point algorithms for estimating power means of positive definite matrices. *IEEE Transactions on Signal Processing*, 65(9):2211–2220.

Cornblath, E. J., Ashourvan, A., Kim, J. Z., Betzel, R. F., Ciric, R., Adebimpe, A., Baum, G. L., He, X., Ruparel, K., Moore, T. M., et al. (2020). Temporal sequences of brain activity at rest are constrained by white matter structure and modulated by cognitive demands. *Communications biology*, 3(1):261.

Cox, R. W. and Hyde, J. S. (1997). Software tools for analysis and visualization of fmri data. *NMR in Biomedicine*, 10(4-5):171–178.

Dale, A. M., Fischl, B., and Sereno, M. I. (1999). Cortical surface-based analysis: I. segmentation and surface reconstruction. *NeuroImage*, 9(2):179–194.

Dam, G., Kording, K., and Wei, K. (2013). Credit assignment during movement reinforcement learning. *PLoS One*, 8(2):e55352.

Daniel, K. (2000). *Thinking fast and slow*. Farrar.

de Brouwer, A. J., Albaghdadi, M., Flanagan, J. R., and Gallivan, J. P. (2018). Using gaze behavior to parcellate the explicit and implicit contributions to visuomotor learning. *Journal of neurophysiology*, 120(4):1602–1615.

de Brouwer, A. J., Areshenkoff, C. N., Rashid, M. R., Flanagan, J. R., Poppenk, J., and Gallivan, J. P. (2022). Human variation in error-based and reinforcement motor learning is associated with entorhinal volume. *Cerebral Cortex*, 32(16):3423–3440.

De Leeuw, J. and Mair, P. (2009). Multidimensional scaling using majorization: Smacof in r. *Journal of statistical software*, 31:1–30.

Diedrichsen, J. (2006). A spatially unbiased atlas template of the human cerebellum. *Neuroimage*, 33(1):127–138.

Doll, B. B., Shohamy, D., and Daw, N. D. (2015). Multiple memory systems as substrates for multiple decision systems. *Neurobiology of learning and memory*, 117:4–13.

Doyon, J., Bellec, P., Amsel, R., Penhune, V., Monchi, O., Carrier, J., Lehéricy, S., and Benali, H. (2009). Contributions of the basal ganglia and functionally related brain structures to motor learning. *Behavioural brain research*, 199(1):61–75.

Drummond, N. M., Cressman, E. K., and Carlsen, A. N. (2015). Inhibition of motor-related activation during a simple reaction time task requiring visuomotor mental rotation. *Behavioral neuroscience*, 129(2):160.

Ellis, N. (1993). Rules and instances in foreign language learning: Interactions of explicit and implicit knowledge. *European Journal of Cognitive Psychology*, 5(3):289–318.

Esteban, O., Blair, R., Markiewicz, C. J., Berleant, S. L., Moodie, C., Ma, F., Isik, A. I., Erramuzpe, A., Kent, James D. andGoncalves, M., DuPre, E., Sitek, K. R., Gomez, D. E. P., Lurie, D. J., Ye, Z., Poldrack, R. A., and Gorgolewski, K. J. (2018a). fmriprep. *Software*.

Esteban, O., Markiewicz, C., Blair, R. W., Moodie, C., Isik, A. I., Erramuzpe Aliaga, A., Kent, J., Goncalves, M., DuPre, E., Snyder, M., Oya, H., Ghosh, S., Wright, J., Durnez, J., Poldrack, R., and Gorgolewski, K. J. (2018b). fMRIPrep: a robust preprocessing pipeline for functional MRI. *Nature Methods*.

Evans, A., Janke, A., Collins, D., and Baillet, S. (2012). Brain templates and atlases. *NeuroImage*, 62(2):911–922.

Fernandez-Ruiz, J., Wong, W., Armstrong, I. T., and Flanagan, J. R. (2011). Relation between reaction time and reach errors during visuomotor adaptation. *Behavioural brain research*, 219(1):8–14.

Filippini, N., Zsoldos, E., Haapakoski, R., Sexton, C. E., Mahmood, A., Allan, C. L., Topiwala, A., Valkanova, V., Brunner, E. J., Shipley, M. J., et al. (2014). Study protocol: the whitehall ii imaging sub-study. *BMC psychiatry*, 14(1):1–16.

Flechsig, P. E. (1920). *Anatomie des menschlichen Gehirns und Rückenmarks auf myelogenetischer Grundlage*, volume 1. G. Thieme.

Fonov, V., Evans, A., McKinstry, R., Almli, C., and Collins, D. (2009). Unbiased nonlinear average age-appropriate brain templates from birth to adulthood. *NeuroImage*, 47, Supplement 1:S102.

Fox, K. C., Spreng, R. N., Ellamil, M., Andrews-Hanna, J. R., and Christoff, K. (2015). The wandering brain: Meta-analysis of functional neuroimaging studies of mind-wandering and related spontaneous thought processes. *Neuroimage*, 111:611–621.

Frazier, J. A., Chiu, S., Breeze, J. L., Makris, N., Lange, N., Kennedy, D. N., Herbert, M. R., Bent, E. K., Koneru, V. K., Dieterich, M. E., et al. (2005). Structural brain magnetic resonance imaging of limbic and thalamic volumes in pediatric bipolar disorder. *American Journal of Psychiatry*, 162(7):1256–1265.

Galea, J. M., Mallia, E., Rothwell, J., and Diedrichsen, J. (2015). The dissociable effects of punishment and reward on motor learning. *Nature neuroscience*, 18(4):597–602.

Glasser, M. F., Coalson, T. S., Robinson, E. C., Hacker, C. D., Harwell, J., Yacoub, E., Ugurbil, K., Andersson, J., Beckmann, C. F., Jenkinson, M., et al. (2016). A multi-modal parcellation of human cerebral cortex. *Nature*, 536(7615):171–178.

Glasser, M. F., Goyal, M. S., Preuss, T. M., Raichle, M. E., and Van Essen, D. C. (2014). Trends and properties of human cerebral cortex: correlations with cortical myelin content. *Neuroimage*, 93:165–175.

Gorgolewski, K., Burns, C. D., Madison, C., Clark, D., Halchenko, Y. O., Waskom, M. L., and Ghosh, S. (2011). Nipype: a flexible, lightweight and extensible neuroimaging data processing framework in python. *Frontiers in Neuroinformatics*, 5:13.

Gorgolewski, K. J., Esteban, O., Markiewicz, C. J., Ziegler, E., Ellis, D. G., Notter, M. P., Jarecka, D., Johnson, H., Burns, C., Manhães-Savio, A., Hamalainen, C., Yvernault, B., Salo, T., Jordan, K., Goncalves, M., Waskom, M., Clark, D., Wong, J., Loney, F., Modat, M., Dewey, B. E., Madison, C., Visconti di Oleggio Castello, M., Clark, M. G., Dayan, M., Clark, D., Keshavan, A., Pinsard, B., Gramfort, A., Berleant, S., Nielson, D. M., Bougacha, S., Varoquaux, G., Cipollini, B., Markello, R., Rokem, A., Moloney, B., Halchenko, Y. O., Wassermann, D., Hanke, M., Horea, C., Kaczmarzyk, J., de Hollander, G., DuPre, E., Gillman, A., Mordom, D., Buchanan, C., Tungaraza, R., Pauli, W. M., Iqbal, S., Sikka, S., Mancini, M., Schwartz, Y., Malone, I. B., Dubois, M., Frohlich, C., Welch, D., Forbes, J., Kent, J., Watanabe, A., Cumba, C., Huntenburg, J. M., Kastman, E., Nichols, B. N., Eshaghi, A., Ginsburg, D., Schaefer, A., Acland, B., Giavasis, S., Kleesiek, J., Erickson, D., Küttner, R., Haselgrove, C., Correa, C., Ghayoor, A., Liem, F., Millman, J., Haehn, D., Lai, J., Zhou, D., Blair, R., Glatard, T., Renfro, M., Liu, S., Kahn, A. E., Pérez-García, F., Triplett, W., Lampe, L., Stadler, J., Kong, X.-Z., Hallquist, M., Chetverikov, A., Salvatore, J., Park, A., Poldrack, R., Craddock, R. C., Inati, S., Hinds, O., Cooper, G., Perkins, L. N., Marina, A., Mattfeld, A., Noel, M., Snoek, L., Matsubara, K., Cheung, B., Rothmei, S., Urchs, S., Durnez, J., Mertz, F., Geisler, D., Floren, A., Gerhard, S., Sharp, P., Molina-Romero, M., Weinstein, A., Broderick, W., Saase, V., Andberg, S. K., Harms, R., Schlamp, K., Arias, J., Papadopoulos Orfanos, D., Tarbert, C., Tambini, A., De La Vega, A., Nickson, T., Brett, M., Falkiewicz, M., Podranski, K., Linkersdörfer, J., Flandin, G., Ort, E., Shachnev, D., McNamee, D., Davison, A., Varada, J., Schwabacher, I., Pellman, J., Perez-Guevara, M., Khanuja, R., Pannetier, N., McDermottroe, C., and Ghosh, S. (2018). Nipype. *Software*.

Gratton, C., Laumann, T. O., Nielsen, A. N., Greene, D. J., Gordon, E. M., Gilmore, A. W., Nelson, S. M., Coalson, R. S., Snyder, A. Z., Schlaggar, B. L., et al. (2018). Functional brain networks are dominated by stable group and individual factors, not cognitive or daily variation. *Neuron*, 98(2):439–452.

Greve, D. N. and Fischl, B. (2009). Accurate and robust brain image alignment using boundary-based registration. *NeuroImage*, 48(1):63–72.

Gugerty, L. J. (1997). Situation awareness during driving: Explicit and implicit knowledge in dynamic spatial memory. *Journal of Experimental Psychology: Applied*, 3(1):42.

Haar, S., Donchin, O., and Dinstein, I. (2015). Dissociating visual and motor directional selectivity using visuomotor adaptation. *Journal of Neuroscience*, 35(17):6813–6821.

Härdle, W. (1990). *Applied nonparametric regression*. Number 19. Cambridge university press.

Hardwick, R. M., Rottschy, C., Miall, R. C., and Eickhoff, S. B. (2013). A quantitative meta-analysis and review of motor learning in the human brain. *Neuroimage*, 67:283–297.

Harmony, T. (2013). The functional significance of delta oscillations in cognitive processing. *Frontiers in integrative neuroscience*, 7:83.

Haruno, M., Wolpert, D. M., and Kawato, M. (1998). Multiple paired forward-inverse models for human motor learning and control. *Advances in neural information processing systems*, 11.

Hasson, U., Chen, J., and Honey, C. J. (2015). Hierarchical process memory: memory as an integral component of information processing. *Trends in cognitive sciences*, 19(6):304–313.

Hasson, U., Yang, E., Vallines, I., Heeger, D. J., and Rubin, N. (2008). A hierarchy of temporal receptive windows in human cortex. *Journal of Neuroscience*, 28(10):2539–2550.

Hawrylycz, M., Miller, J. A., Menon, V., Feng, D., Dolbeare, T., Guillozet-Bongaarts, A. L., Jegga, A. G., Aronow, B. J., Lee, C.-K., Bernard, A., et al. (2015). Canonical genetic signatures of the adult human brain. *Nature neuroscience*, 18(12):1832–1844.

Hegele, M. and Heuer, H. (2010). Implicit and explicit components of dual adaptation to visuomotor rotations. *Consciousness and cognition*, 19(4):906–917.

Heuer, H. and Hegele, M. (2008). Constraints on visuo-motor adaptation depend on the type of visual feedback during practice. *Experimental Brain Research*, 185:101–110.

Hill, J., Inder, T., Neil, J., Dierker, D., Harwell, J., and Van Essen, D. (2010). Similar patterns of cortical expansion during human development and evolution. *Proceedings of the National Academy of Sciences*, 107(29):13135–13140.

Holland, P., Codol, O., and Galea, J. M. (2018). Contribution of explicit processes to reinforcement-based motor learning. *Journal of neurophysiology*, 119(6):2241–2255.

Huntenburg, J. M., Bazin, P.-L., Goulas, A., Tardif, C. L., Villringer, A., and Margulies, D. S. (2017). A systematic relationship between functional connectivity and intracortical myelin in the human cerebral cortex. *Cerebral Cortex*, 27(2):981–997.

Huntenburg, J. M., Bazin, P.-L., and Margulies, D. S. (2018). Large-scale gradients in human cortical organization. *Trends in cognitive sciences*, 22(1):21–31.

Izawa, J. and Shadmehr, R. (2011). Learning from sensory and reward prediction errors during motor adaptation. *PLoS computational biology*, 7(3):e1002012.

Jenkinson, M., Bannister, P., Brady, M., and Smith, S. (2002). Improved optimization for the robust and accurate linear registration and motion correction of brain images. *NeuroImage*, 17(2):825–841.

Keisler, A. and Shadmehr, R. (2010). A shared resource between declarative memory and motor memory. *Journal of Neuroscience*, 30(44):14817–14823.

Kim, S., Ogawa, K., Lv, J., Schweighofer, N., and Imamizu, H. (2015). Neural substrates related to motor memory with multiple timescales in sensorimotor adaptation. *PLoS biology*, 13(12):e1002312.

Klein, A., Ghosh, S. S., Bao, F. S., Giard, J., Häme, Y., Stavsky, E., Lee, N., Rossa, B., Reuter, M., Neto, E. C., and Keshavan, A. (2017). Mindboggling morphometry of human brains. *PLOS Computational Biology*, 13(2):e1005350.

Konishi, M., McLaren, D. G., Engen, H., and Smallwood, J. (2015). Shaped by the past: the default mode network supports cognition that is independent of immediate perceptual input. *PloS one*, 10(6):e0132209.

Krakauer, J. W. (2009). Motor learning and consolidation: the case of visuomotor rotation. *Progress in motor control*, pages 405–421.

Kumaran, D., Summerfield, J. J., Hassabis, D., and Maguire, E. A. (2009). Tracking the emergence of conceptual knowledge during human decision making. *Neuron*, 63(6):889–901.

Lanczos, C. (1964). Evaluation of noisy data. *Journal of the Society for Industrial and Applied Mathematics Series B Numerical Analysis*, 1(1):76–85.

Ledoit, O. and Wolf, M. (2004). A well-conditioned estimator for large-dimensional covariance matrices. *Journal of multivariate analysis*, 88(2):365–411.

Lee, S. W., O'Doherty, J. P., and Shimojo, S. (2015). Neural computations mediating one-shot learning in the human brain. *PLoS biology*, 13(4):e1002137.

Liew, S.-L., Thompson, T., Ramirez, J., Butcher, P. A., Taylor, J. A., and Celnik, P. A. (2018). Variable neural contributions to explicit and implicit learning during visuomotor adaptation. *Frontiers in neuroscience*, 12:610.

Ludyga, S., Pühse, U., Gerber, M., and Herrmann, C. (2019). Core executive functions are selectively related to different facets of motor competence in preadolescent children. *European journal of sport science*, 19(3):375–383.

Makris, N., Goldstein, J. M., Kennedy, D., Hodge, S. M., Caviness, V. S., Faraone, S. V., Tsuang, M. T., and Seidman, L. J. (2006). Decreased volume of left and total anterior insular lobule in schizophrenia. *Schizophrenia research*, 83(2-3):155–171.

Manto, M., Bower, J. M., Conforto, A. B., Delgado-García, J. M., Da Guarda, S. N. F., Gerwig, M., Habas, C., Hagura, N., Ivry, R. B., Mariën, P., et al. (2012). Consensus paper: roles of the cerebellum in motor control—the diversity of ideas on cerebellar involvement in movement. *The Cerebellum*, 11:457–487.

Margulies, D. S., Ghosh, S. S., Goulas, A., Falkiewicz, M., Huntenburg, J. M., Langs, G., Bezgin, G., Eickhoff, S. B., Castellanos, F. X., Petrides, M., et al. (2016). Situating the default-mode network along a principal gradient of macroscale cortical organization. *Proceedings of the National Academy of Sciences*, 113(44):12574–12579.

Markello, R. D., Hansen, J. Y., Liu, Z.-Q., Bazinet, V., Shafiei, G., Suárez, L. E., Blostein, N., Seidlitz, J., Baillet, S., Satterthwaite, T. D., et al. (2022). Neuromaps: structural and functional interpretation of brain maps. *Nature Methods*, 19(11):1472–1479.

Martin, R., Tigera, C., Denckla, M. B., and Mark Mahone, E. (2010). Factor structure of paediatric timed motor examination and its relationship with iq. *Developmental Medicine & Child Neurology*, 52(8):e188–e194.

Mazzoni, P. and Krakauer, J. W. (2006). An implicit plan overrides an explicit strategy during visuomotor adaptation. *Journal of neuroscience*, 26(14):3642–3645.

McInnes, L., Healy, J., and Melville, J. (2018). Umap: Uniform manifold approximation and projection for dimension reduction. *arXiv preprint arXiv:1802.03426*.

Mesulam, M.-M. (1998). From sensation to cognition. *Brain: a journal of neurology*, 121(6):1013–1052.

Murphy, C., Jefferies, E., Rueschemeyer, S.-A., Sormaz, M., Wang, H.-t., Margulies, D. S., and Smallwood, J. (2018). Distant from input: Evidence of regions within the default mode network supporting perceptually-decoupled and conceptually-guided cognition. *Neuroimage*, 171:393–401.

Murphy, C., Wang, H.-T., Konu, D., Lowndes, R., Margulies, D. S., Jefferies, E., and Smallwood, J. (2019). Modes of operation: A topographic neural gradient supporting stimulus dependent and independent cognition. *NeuroImage*, 186:487–496.

Oldfield, N. (1971). Edinburgh handedness questionnaire. *Neuropsychologia*, 9:97–113.

Paquola, C., Amunts, K., Evans, A., Smallwood, J., and Bernhardt, B. (2022). Closing the mechanistic gap: the value of microarchitecture in understanding cognitive networks. *Trends in Cognitive Sciences*.

Paquola, C., Bethlehem, R. A., Seidlitz, J., Wagstyl, K., Romero-Garcia, R., Whitaker, K. J., Vos de Wael, R., Williams, G. B., Consortium, N., Vértes, P. E., et al. (2019). Shifts in myeloarchitecture characterise adolescent development of cortical gradients. *elife*, 8:e50482.

Paulus, M. P., Hozack, N., Zauscher, B., McDowell, J. E., Frank, L., Brown, G. G., and Braff, D. L. (2001). Prefrontal, parietal, and temporal cortex networks underlie decision-making in the presence of uncertainty. *Neuroimage*, 13(1):91–100.

Pearson, J. M., Hayden, B. Y., and Platt, M. L. (2011a). A role for posterior cingulate cortex in policy switching and cognitive control. *Neural Basis of Motivational and Cognitive Control*, page 127.

Pearson, J. M., Hayden, B. Y., Raghavachari, S., and Platt, M. L. (2009). Neurons in posterior cingulate cortex signal exploratory decisions in a dynamic multioption choice task. *Current biology*, 19(18):1532–1537.

Pearson, J. M., Heilbronner, S. R., Barack, D. L., Hayden, B. Y., and Platt, M. L. (2011b). Posterior cingulate cortex: adapting behavior to a changing world. *Trends in cognitive sciences*, 15(4):143–151.

Pearson, K. and Filon, L. N. G. (1898). Vii. mathematical contributions to the theory of evolution.—iv. on the probable errors of frequency constants and on the influence of random selection on variation and correlation. *Philosophical Transactions of the Royal Society of London. Series A, Containing Papers of a Mathematical or Physical Character*, (191):229–311.

Piek, J. P., Dyck, M. J., Nieman, A., Anderson, M., Hay, D., Smith, L. M., McCoy, M., and Hallmayer, J. (2004). The relationship between motor coordination, executive functioning and attention in school aged children. *Archives of clinical Neuropsychology*, 19(8):1063–1076.

Power, J. D., Mitra, A., Laumann, T. O., Snyder, A. Z., Schlaggar, B. L., and Petersen, S. E. (2014). Methods to detect, characterize, and remove motion artifact in resting state fmri. *NeuroImage*, 84(Supplement C):320–341.

Pruim, R. H. R., Mennes, M., van Rooij, D., Llera, A., Buitelaar, J. K., and Beckmann, C. F. (2015). Ica-AROMA: A robust ICA-based strategy for removing motion artifacts from fmri data. *NeuroImage*, 112(Supplement C):267–277.

Ramsay, J., Wickham, H., Ramsay, M. J., and deSolve, S. (2022). Package 'fda'.

Reineberg, A. E., Andrews-Hanna, J. R., Depue, B. E., Friedman, N. P., and Banich, M. T. (2015). Resting-state networks predict individual differences in common and specific aspects of executive function. *Neuroimage*, 104:69–78.

Reuter, M., Rosas, H. D., and Fischl, B. (2010). Highly accurate inverse consistent registration: A robust approach. *NeuroImage*, 53(4):1181–1196.

Satterthwaite, T. D., Elliott, M. A., Gerraty, R. T., Ruparel, K., Loughead, J., Calkins, M. E., Eickhoff, S. B., Hakonarson, H., Gur, R. C., Gur, R. E., and Wolf, D. H. (2013). An improved framework for confound regression and filtering for control of motion artifact in the preprocessing of resting-state functional connectivity data. *NeuroImage*, 64(1):240–256.

Schaefer, A., Kong, R., Gordon, E. M., Laumann, T. O., Zuo, X.-N., Holmes, A. J., Eickhoff, S. B., and Yeo, B. T. (2018). Local-global parcellation of the human cerebral cortex from intrinsic functional connectivity mri. *Cerebral cortex*, 28(9):3095–3114.

Schendan, H. E., Searl, M. M., Melrose, R. J., and Stern, C. E. (2003). An fmri study of the role of the medial temporal lobe in implicit and explicit sequence learning. *Neuron*, 37(6):1013–1025.

Scott, S. H. (2004). Optimal feedback control and the neural basis of volitional motor control. *Nature Reviews Neuroscience*, 5(7):532–545.

Scott, S. H. (2012). The computational and neural basis of voluntary motor control and planning. *Trends in cognitive sciences*, 16(11):541–549.

Shang, H. L. (2014). A survey of functional principal component analysis. *AStA Advances in Statistical Analysis*, 98(2):121–142.

Smallwood, J., Bernhardt, B. C., Leech, R., Bzdok, D., Jefferies, E., and Margulies, D. S. (2021). The default mode network in cognition: a topographical perspective. *Nature reviews neuroscience*, 22(8):503–513.

Smith, M. A., Ghazizadeh, A., and Shadmehr, R. (2006). Interacting adaptive processes with different timescales underlie short-term motor learning. *PLoS biology*, 4(6):e179.

Spreng, R. N., Mar, R. A., and Kim, A. S. (2009). The common neural basis of autobiographical memory, prospection, navigation, theory of mind, and the default mode: a quantitative meta-analysis. *Journal of cognitive neuroscience*, 21(3):489–510.

Stan Development Team (2022). RStan: the R interface to Stan. R package version 2.21.5.

Stark-Inbar, A., Raza, M., Taylor, J. A., and Ivry, R. B. (2017). Individual differences in implicit motor learning: task specificity in sensorimotor adaptation and sequence learning. *Journal of neurophysiology*, 117(1):412–428.

Stüber, C., Morawski, M., Schäfer, A., Labadie, C., Wähnert, M., Leuze, C., Streicher, M., Barapatre, N., Reimann, K., Geyer, S., et al. (2014). Myelin and iron concentration in the human brain: a quantitative study of mri contrast. *Neuroimage*, 93:95–106.

Sutton, R. S. and Barto, A. G. (2018). *Reinforcement learning: An introduction*. MIT press.

Tanaka, H., Ishikawa, T., Lee, J., and Kakei, S. (2020). The cerebro-cerebellum as a locus of forward model: a review. *Frontiers in systems neuroscience*, 14:19.

Taylor, J. A. and Ivry, R. B. (2011). Flexible cognitive strategies during motor learning. *PLoS computational biology*, 7(3):e1001096.

Taylor, J. A. and Ivry, R. B. (2012). The role of strategies in motor learning. *Annals of the New York Academy of Sciences*, 1251(1):1–12.

Taylor, J. A., Klemfuss, N. M., and Ivry, R. B. (2010). An explicit strategy prevails when the cerebellum fails to compute movement errors. *The Cerebellum*, 9:580–586.

Taylor, J. A., Krakauer, J. W., and Ivry, R. B. (2014). Explicit and implicit contributions to learning in a sensorimotor adaptation task. *Journal of Neuroscience*, 34(8):3023–3032.

Teissier, A. and Pierani, A. (2021). Wiring of higher-order cortical areas: Spatiotemporal development of cortical hierarchy. In *Seminars in Cell & Developmental Biology*, volume 118, pages 35–49. Elsevier.

Therrien, A. S., Wolpert, D. M., and Bastian, A. J. (2016). Effective reinforcement learning following cerebellar damage requires a balance between exploration and motor noise. *Brain*, 139(1):101–114.

Tseng, Y.-w., Diedrichsen, J., Krakauer, J. W., Shadmehr, R., and Bastian, A. J. (2007). Sensory prediction errors drive cerebellum-dependent adaptation of reaching. *Journal of neurophysiology*, 98(1):54–62.

Tustison, N. J., Avants, B. B., Cook, P. A., Zheng, Y., Egan, A., Yushkevich, P. A., and Gee, J. C. (2010). N4itk: Improved n3 bias correction. *IEEE Transactions on Medical Imaging*, 29(6):1310–1320.

Van De Wiel, M. A., Lien, T. G., Verlaat, W., van Wieringen, W. N., and Wilting, S. M. (2016). Better prediction by use of co-data: adaptive group-regularized ridge regression. *Statistics in medicine*, 35(3):368–381.

van de Wiel, M. A. and Novianti, P. W. (2022). *GRridge: Better prediction by use of co-data: Adaptive group-regularized ridge regression*. R package version 1.22.0.

Wolpert, D. M. (1997). Computational approaches to motor control. *Trends in cognitive sciences*, 1(6):209–216.

Wolpert, D. M., Diedrichsen, J., and Flanagan, J. R. (2011). Principles of sensorimotor learning. *Nature reviews neuroscience*, 12(12):739–751.

Wu, H. G., Miyamoto, Y. R., Castro, L. N. G., Ölveczky, B. P., and Smith, M. A. (2014). Temporal structure of motor variability is dynamically regulated and predicts motor learning ability. *Nature neuroscience*, 17(2):312–321.

Yeo, B. T., Krienen, F. M., Sepulcre, J., Sabuncu, M. R., Lashkari, D., Hollinshead, M., Roffman, J. L., Smoller, J. W., Zöllei, L., Polimeni, J. R., et al. (2011). The organization of the human cerebral cortex estimated by intrinsic functional connectivity. *Journal of neurophysiology*.

Zhang, M., Bernhardt, B. C., Wang, X., Varga, D., Krieger-Redwood, K., Royer, J., Rodríguez-Cruces, R., de Wael, R. V., Margulies, D. S., Smallwood, J., et al. (2022). Perceptual coupling and decoupling of the default mode network during mind-wandering and reading. *Elife*, 11:e74011.

Zhang, M., Savill, N., Margulies, D. S., Smallwood, J., and Jefferies, E. (2019). Distinct individual differences in default mode network connectivity relate to off-task thought and text memory during reading. *Scientific reports*, 9(1):1–13.

Zhang, Y., Brady, M., and Smith, S. (2001). Segmentation of brain MR images through a hidden markov random field model and the expectation-maximization algorithm. *IEEE Transactions on Medical Imaging*, 20(1):45–57.

Zhao, Q., Kwon, D., and Pohl, K. M. (2018). A riemannian framework for longitudinal analysis of resting-state functional connectivity. In *International Conference on Medical Image Computing and Computer-Assisted Intervention*, pages 145–153. Springer.

4 Supplemental figures

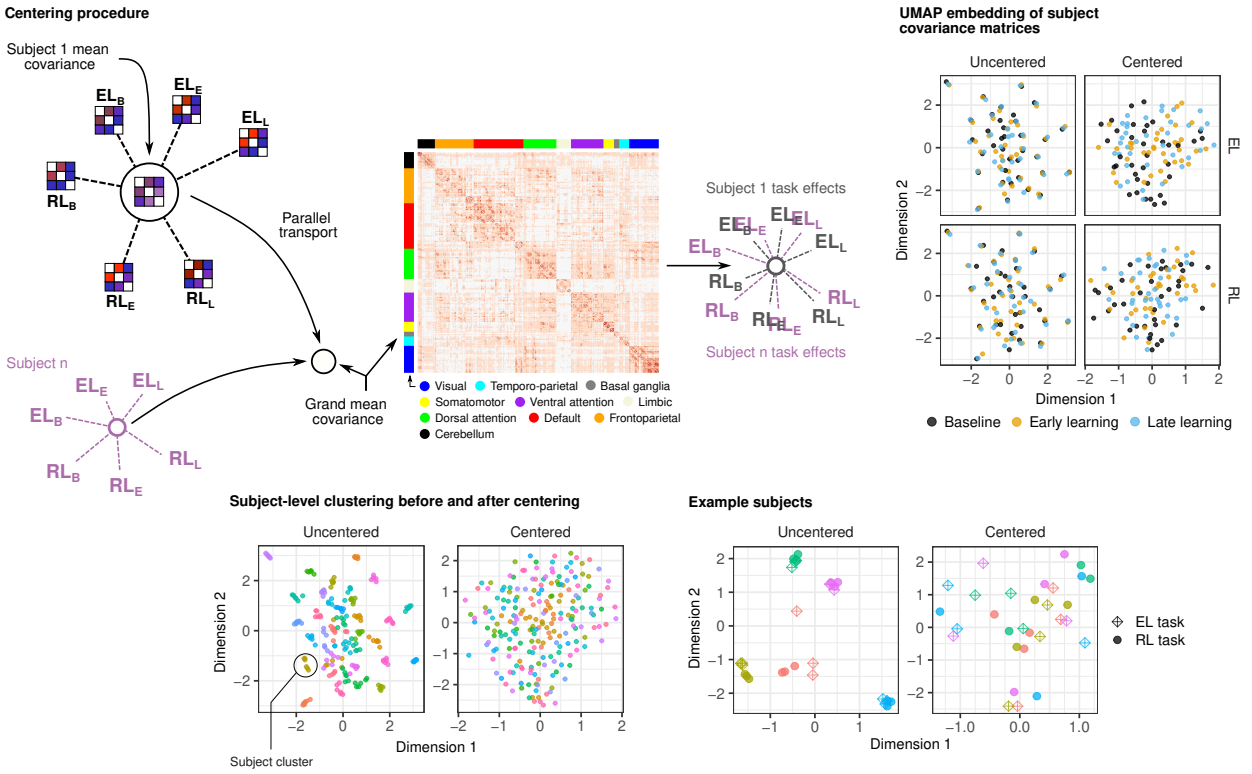

Figure 8: **Effects of covariance centering procedure –** Subject's covariance matrices – extracted during baseline, early, and late learning – were centered to align each subject's mean covariance to the grand mean covariance across all subjects (see Methods). To visualize the effects of this centering procedure, we applied uniform manifold approximation (UMAP; McInnes et al., 2018) to the matrix of geodesic distances between covariance matrices in order to derive a two-dimensional embedding both before and after centering. The results of this embedding, for each task, are seen in the top right panel. In the bottom left – colored by subject – we see strong subject-level clustering before centering, consistent with the findings of Gratton et al. (2018) that task-related changes in functional connectivity are relatively small compared to static, subject-level differences. Note that this subject-level clustering is abolished by our centering procedure.

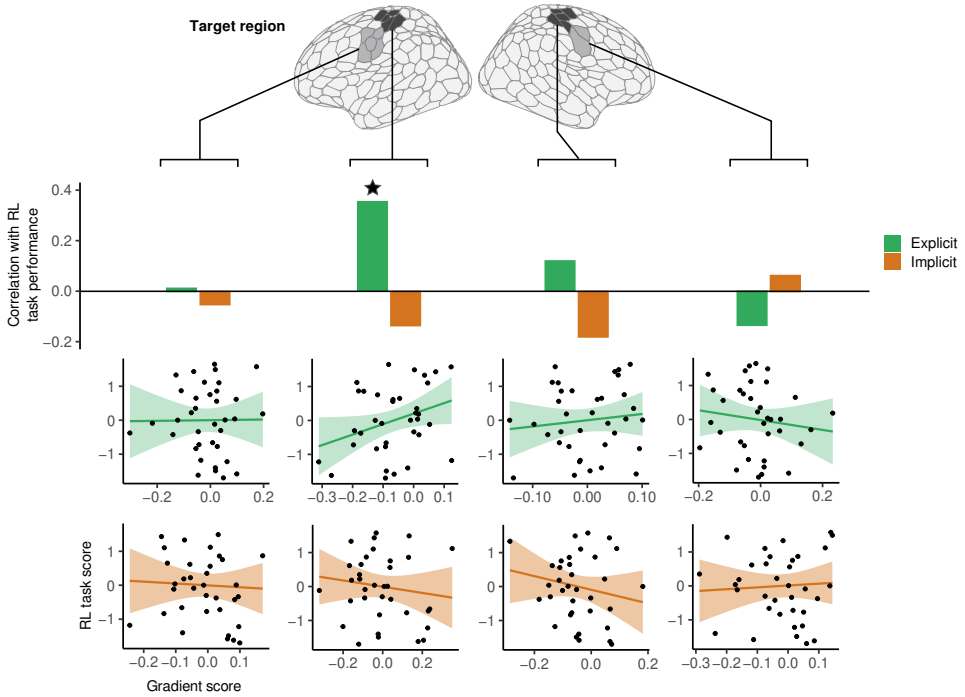

Figure 9: **Correlation of implicit/explicit gradient scores with performance I –** Scatterplots show the association between implicit and explicit gradient scores – derived during the early learning epoch of the EL task – and RL task scores. Results are shown for the contra- and ipsilateral motor cortices, separately for hand an tongue areas.

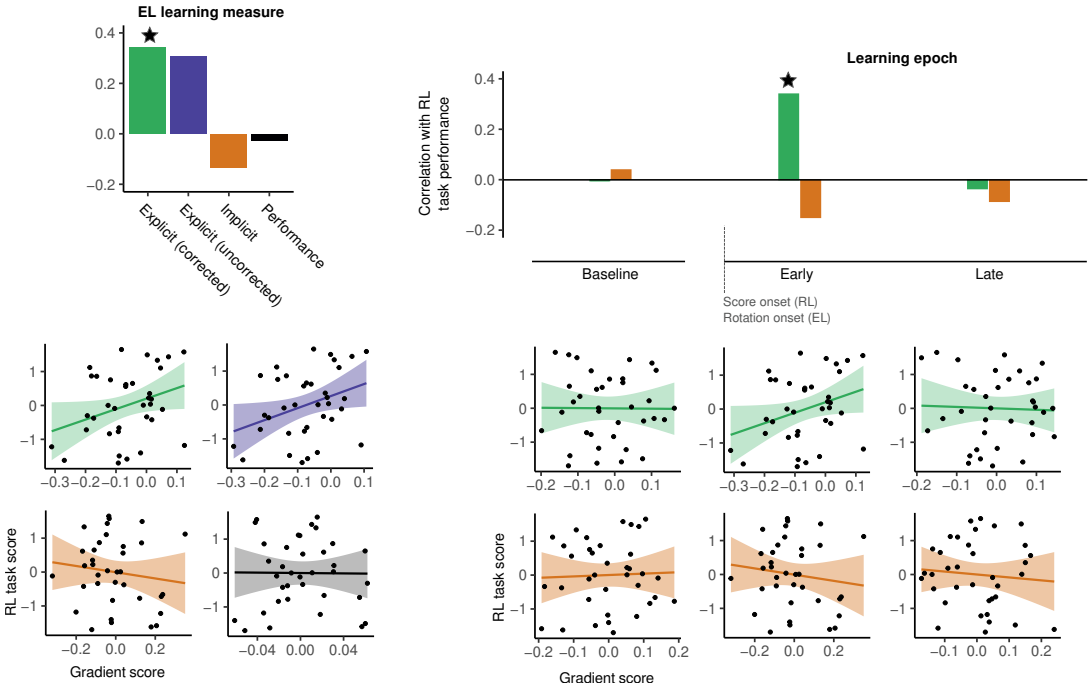

Figure 10: **Correlation of implicit/explicit gradient scores with performance II –** Scatterplots show the association between gradient scores – derived during different EL task epochs– and RL task scores. Results are shown for gradients derived during the early learning epoch from explicit learning scores (corrected and uncorrected for EL task performance), implicit learning scores, and for EL task performance (left). At the right, we show effects for implicit and explicit gradients derived from each phase of the EL task.